

The Use of Theoretical Models to Improve Global Maps of foF2

C.M. Rush
M. PoKempner
D.N. Anderson
F.G. Stewart



U.S. DEPARTMENT OF COMMERCE
Malcolm Baldrige, Secretary

Bernard J. Wunder, Jr., Assistant Secretary
for Communications and Information

January 1982



TABLE OF CONTENTS

	<u>PAGE</u>
LIST OF FIGURES	v
LIST OF TABLES	vii
ABSTRACT	1
1. INTRODUCTION	1
2. THEORETICAL CONSIDERATIONS	3
2.1 Neutral Atmosphere Model	4
2.2 Production and Loss Rate	6
2.3 Diffusion Coefficient	6
2.4 Neutral Wind Models	6
2.5 Electrodynamical Drift Velocity Models	7
2.6 Geomagnetic Field Model	7
2.7 Solution to the Full Continuity Equation	7
3. METHOD OF ANALYSIS	14
3.1 Mathematical Basis	14
3.1.1 Diurnal analysis	15
3.1.2 Geographic analysis	16
3.2 Data Used in Constructing Maps	19
4. RESULTS OF THE GLOBAL REPRESENTATIONS OF foF2 USING THE THEORETICAL foF2 VALUES	21
5. DISCUSSION AND CONCLUSION	37
6. ACKNOWLEDGMENT	40
7. REFERENCES	40

LIST OF FIGURES

<u>FIGURE</u>		<u>PAGE</u>
1.	Meridional and zonal neutral wind model for the Southern Hemisphere for September 1978.	8
2.	Meridional and zonal neutral wind model for the Southern Hemisphere for December 1978.	9
3.	Comparison between median values of foF2 observed at Auckland, New Zealand and values calculated using the theoretical model for September 1978.	11
4.	Diurnal behavior of foF2 during September 1978 deduced using the theoretical model with the same neutral wind model at three locations in the Southern Hemisphere having essentially the same dip but different declinations.	12
5.	Diurnal behavior of foF2 during December 1978 deduced using the theoretical model with the same neutral wind model at three locations in the Southern Hemisphere having essentially the same dip but different declinations.	13
6.	Global distribution of data points used to generate maps of foF2 for December 1975. The two heavy lines shown on the Figure are the locations of the 0° declination.	22
7.	Contour map of the global representation of the median value of foF2 for December 1975 at 06 UT.	23
8.	Contour map of the global representation of the median value of foF2 for December 1975 at 18 UT.	24
9.	Contour map of the global representation of the median value of foF2 for December 1978 at 06 UT.	25
10.	Contour map of the global representation of the median value of foF2 for December 1978 at 18 UT.	26
11.	Longitudinal distribution of foF2 at 30°, 40°, and 50° south latitude for December 1978 at 10 UT.	28
12.	Comparison between the diurnal variation of foF2 observed at Kerguelen during September 1978 with that deduced from the theoretical calculations and the CCIR coefficients.	29
13.	Comparison between the diurnal variation of foF2 observed at Kerguelen during December 1978 with that deduced from the theoretical calculations and the CCIR coefficients.	30

LIST OF FIGURES (Continued)

<u>FIGURE</u>		<u>PAGE</u>
14.	Comparison between the diurnal variation of foF2 for December 1975 and December 1978 deduced from the existing CCIR coefficients, the new coefficients developed in this study, and from the theoretical model or from observations where available. Plots are shown for observations at Brisbane, Norfolk Island, and Falkland Island and theoretical calculations at points 16, 19, and 20.	32
15.	Comparison between the diurnal variation of foF2 for December 1975 and December 1978 deduced from the existing CCIR coefficients, the new coefficients developed in this study, and from the theoretical model or from observations where available. Plots are shown for observations at Mundaring, Canberra, Auckland, and Christchurch and theoretical calculations at points 31 and 33.	33
16.	Comparison between the diurnal variation of foF2 for December 1975 and December 1978 deduced from the existing CCIR coefficients, the new coefficients developed in this study, and from the theoretical model or from observations where available. Plots are shown for observations at Kerguelen, Hobart, Campbell Island, and Argentine Island and theoretical calculations at points 57 and 60.	36
17.	Comparison between the diurnal variation of foF2 for July 1975 and September 1978 deduced from the existing CCIR coefficients, the new coefficients developed in this study, and from the theoretical model for points 19, 20, 31, and 60.	38

LIST OF TABLES

<u>TABLE</u>		<u>PAGE</u>
1.	Input parameters for the time-dependent ion continuity equation.	5
2.	Set of functions chosen to represent the geographic variation of the Fourier coefficients.	17
3.	Location of A stations and D points used to illustrate diurnal behavior of foF2	34

THE USE OF THEORETICAL MODELS TO IMPROVE GLOBAL MAPS OF foF2

Charles M. Rush*, Margo PoKempner**, David N. Anderson***, and F. G. Stewart*

In this report, the results of a study to improve the global maps of monthly median values of the F2 region critical frequency, foF2, using values determined from a theoretical model, are presented. The object of the study was to obtain values of the mid-latitude F-region critical frequency which could be used to improve the prediction of ionospheric parameters in regions of the earth inaccessible to ground-based measurements. This was accomplished by including, into the theoretical calculations, realistic physical processes along with a realistic geomagnetic field model. Parameters were adjusted so that agreement was achieved between calculated and observed foF2 values as a function of local time at different stations and then these same input parameters (i.e., neutral wind field, neutral atmospheric model, electrodynamic drift) were assumed valid at all regions of interest where the major difference is the geomagnetic field-line configuration. Coefficients that yield global representations of foF2 were then determined using the theoretically derived foF2 values, and the predicted critical frequencies were compared with observed values to estimate the degree of improvement.

Key words: foF2, ionospheric mapping, neutral winds,
time-dependent continuity equation

1. INTRODUCTION

Global maps of monthly median ionospheric parameters published by the International Radio Consultative Committee (CCIR) form the basis for a number of empirical and statistical models of the ionospheric electron density (CCIR, 1978a). The accuracy of such models is therefore tied directly to the accuracy of the maps of the ionospheric parameters. Maps of the critical frequency of the E region, foE (Leftin, 1976), the critical frequency of the F1 region, foF1 (Rosich and Jones, 1973), and the critical frequency of the F2 region, foF2 (Jones et al., 1969; Jones and Obitts, 1970) have been employed in one form or another to determine ionospheric structure (Nisbet, 1971), HF propagation conditions (Barghausen et al., 1969; CCIR, 1978b), and transionospheric propagation factors (Bent et al., 1978). Studies have

* Charles Rush and F.G. Stewart are with the U.S. Department of Commerce, National Telecommunications and Information Administration, Institute for Telecommunication Sciences, Boulder, Colorado.

** Margo PoKempner is with OAO, Boulder, Colorado.

***David N. Anderson is with the National Oceanic and Atmospheric Administration, Space Environment Laboratory, Boulder, Colorado.

been reported (Zevakina et al., 1967 and Rush, 1978) describing how the global maps of monthly median ionospheric parameters can be modified with daily ionospheric observations in order to represent more realistically the daily variations in ionospheric structure.

The global maps of ionospheric parameters are generated from numerical coefficients obtained by performing a spherical harmonic analysis on observed monthly median values of foE, foF1, and foF2. The basis for the analysis has been described in detail by Jones and Gallet (1962). The resultant accuracy of the maps depends on the geographical distribution of the data that were used in the generation of the coefficients. The data, foE, foF1, and foF2, that were used in developing the global maps were obtained from between 100 and 150 vertical incidence ionosonde stations that operated throughout the world. These stations provided observations that permit generating a reasonably accurate map of the ionospheric parameters at those locations for which data were available. At locations for which data were non-existent, such as for ocean areas, the accuracy of the maps is questionable.

It has long been appreciated that the uncertainties in the maps of foF2 are the largest potential source of error in any ionospheric model that uses global maps of median ionospheric parameters. This is principally due to the fact that of the ionospheric regions for which maps are available, the F2 region is the most variable (see Rush and Gibbs 1973), displaying large changes on both temporal and spatial scales. The variations in the F2 region are the manifestation of complex interactions between neutral and ionized constituents, the dependence of F2 region phenomena upon the geomagnetic field, and the influence of the magnetosphere on the ionosphere. The variability of the F2 region renders it difficult to extrapolate observations of foF2 at one location to another location with a degree of accuracy that is commensurate with extrapolation procedures employed for the E and F1 regions. In order to rectify this situation somewhat, it was decided to employ a theoretical model of the ionosphere to generate values of the F2 region critical frequency in low and mid-latitude parts of the world including locations where observations of foF2 are unavailable. The values of foF2 determined from the theoretical model were then combined with actual observations of foF2 and, in some instances, with values of foF2 determined from the coefficients described by Jones and Obitts (1970). These data then formed the basis for re-generating the numerical coefficients that yield global maps of the F2 region critical frequency for specific months. The resultant maps provide a means to specify foF2 on a global basis that is consistent with observation and with the physical understanding about the structures of the low and mid-latitude F2 region and the causes of its large-scale variations.

The purpose of this report is to present the results of the study mentioned above along with a description of the methods that were employed to generate theoretical values of the F2 region critical frequency. In the next section, the methods used to generate these values of foF2 are described. The theoretical values of foF2 were determined from the time-dependent continuity equation for ions and electrons in the ionosphere and procedures were adopted to assure that the theoretically calculated values were consistent with available observed values of foF2. In the third section of this report, the methods employed to generate new coefficients and ionospheric maps are described. In addition to providing the mathematical basis for the analysis that was undertaken, Section 3 provides a discussion of the observed data that were used as well as the data calculated using the Jones-Obitts coefficients. In Section 4, the results of the present study are presented and a discussion concerning the accuracy of the maps is provided. Finally, in Section 5, the overall conclusions derived from this investigation are delineated along with areas where further study is warranted.

2. THEORETICAL CONSIDERATIONS

The theoretical values of the F2 region critical frequency at low and mid-latitudes were obtained by use of the time-dependent ion continuity equation as described by Anderson (1973). Because the positive ion density (N_i) is equal to the electron density (N_e) at the altitudes of interest, values obtained from the time-dependent ion continuity equation can be used to determine foF2 directly using the relationship

$$N_e \left(\frac{e1}{\text{cm}^3} \right) = 1.24 \times 10^4 (\text{foF2})^2 \quad (1)$$

where foF2 is in MHz.

In arriving at the solution to the continuity equation, it was assumed that the only ion of concern was atomic oxygen (O^+), which is a valid approximation for F2 region heights.

To find the ion (O^+) and electron density as a function of altitude, latitude, and local time, the time-dependent ion continuity equation including the effects of production, loss by charge exchange, and transport by diffusion, neutral wind, and electrodynamic ($\bar{E} \times \bar{B}$) drift was numerically solved.

The continuity equation is given by

$$\partial N_i / \partial t + \nabla \cdot (N_i \bar{V}_i) = P_i - L_i \quad (2)$$

where N_i is the ion density; P_i , the ion production rate; L_i , the loss rate; and \bar{V}_i , the transport velocity. In the ionosphere, plasma is transported along the geomagnetic field lines by diffusion and neutral winds and perpendicular to field lines primarily by electrodynamic $\bar{E} \times \bar{B}$ drift (Kendall and Pickering, 1967). In solving (2), the independent coordinates are transformed to a coordinate system parallel and perpendicular to the magnetic field line (see Anderson, 1973). Equation (2) can then be written

$$\partial N_i / \partial t + \bar{V}_{i\perp} \cdot \nabla N_i = P_i - L_i - \nabla \cdot (N_i \bar{V}_{i\parallel}) - N_i \nabla \cdot \bar{V}_{i\perp} \quad (3)$$

where $\bar{V}_{i\perp}$ is given by $\bar{E} \times \bar{B} / B^2$ and $\bar{V}_{i\parallel}$ includes the effects of plasma diffusion and neutral wind. The left hand side of (3) is the time rate-of-change of the ion density in a reference frame moving with the electrodynamic drift and is such that the plasma simply co-rotates with the earth, $\nabla \cdot \bar{V}_{i\perp} = 0$. The right side of (3) involves terms which are second order in the coordinate parallel to B . Equation (3) is solved numerically, (see Anderson, 1973 for details) to give N_i ($=N_e$) densities as a function of altitude, latitude, and local time.

The set of coefficients for the ion continuity equation was obtained from models of the neutral composition; neutral temperature; ion and electron temperatures; and production, loss, and diffusion rates, as well as the neutral wind model, electrodynamic drift model, and geomagnetic field model. Calculations were performed for the months of July, September, and December of 1975 and 1978 using appropriate solar and geophysical indices. A brief description of these models is given below.

2.1 Neutral Atmosphere Model

The neutral atmospheric model derived from mass spectrometer and incoherent scatter data designated as the MSIS model (Hedin et al., 1977) was used to calculate the density of nitrogen (N_2), molecular oxygen (O_2), and atomic oxygen (O) and the neutral temperature, T , as a function of altitude, latitude, and local time. At all altitudes and local times, it was assumed that the ionosphere was in thermal equilibrium with the neutral (T_n), ion (T_i) and electron (T_e) temperatures being equal. Values of N_2 , O_2 , and O and T_n were obtained as a function of altitude, latitude, and local time for specific solar flux conditions. The solar flux values (and corresponding mean Zurich sunspot number R) for the months and years used in this study are given in Table 1.

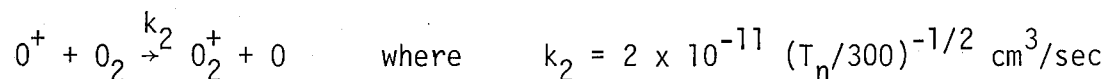
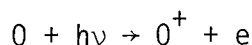
TABLE 1

Input parameters for the time-dependent ion continuity equation

Month	Solar Flux at 10.7 cm	R, Zurich Sunspot Number	Rate of Ion ₁ Production P (sec ⁻¹)
July 1975	77	15	2.3×10^{-7}
September 1975	77	15	2.3×10^{-7}
December 1975	77	16	2.3×10^{-7}
July 1978	150	95	4.0×10^{-7}
September 1978	160	108	4.0×10^{-7}
December 1978	165	117	4.5×10^{-7}

2.2 Production and Loss Rate

The production rate and loss rate reactions incorporated in the calculations of the O^+ densities were similar to those given by Anderson (1973), viz



The value of the photoionization coefficient at the top of the atmosphere, P , was varied according to the solar/geophysical conditions appropriate for each month and is also given in Table 1.

2.3 Diffusion Coefficient

The diffusion coefficient for elastic collisions between ions and neutrals is given by (Anderson, 1973):

$$D_{in}^{-1} = \frac{300}{T_n} \left[\frac{[O_2]}{\sigma O_2} + \frac{[N_2]}{\sigma N_2} + \frac{[O]}{\sigma O} \right]$$

where

$$\sigma O_2 = 3.3 \times 10^{18} \text{ cm}^{-1} \text{ sec}^{-1},$$

$$\sigma N_2 = 3.9 \times 10^{18} \text{ cm}^{-1} \text{ sec}^{-1},$$

and

$$\sigma O = 3.7 \times 10^{18} \text{ cm}^{-1} \text{ sec}^{-1}.$$

The terms $[O_2]$, $[N_2]$, and $[O]$ represent the number densities of molecular oxygen, molecular nitrogen, and atomic oxygen, respectively. These values, along with T_n , the neutral temperature, were derived from the neutral atmosphere model.

2.4 Neutral Wind Models

Values of meridional and zonal neutral-air winds for each of the months were deduced by fitting theoretically calculated values of foF2 to actual monthly median observations at specific mid-latitude locations. The continuity equation was used to calculate hourly values of foF2 for a location where foF2 observations were available and the meridional component of the wind was adjusted so that agreement between observed and calculated values were obtained. The calculation was then repeated for

a location where the foF2 data were available and where the magnetic latitude was essentially the same as for the first calculation but the declination of the geomagnetic field was vastly different. Using the same meridional wind, the zonal wind component was adjusted so that calculated values of foF2 agreed with observations at the second location.

Meridional and zonal neutral wind models were determined for each of the months July, September, and December for both 1975 and 1978. Different models for the same months were obtained for the northern and southern hemispheres of the globe. Figures 1 and 2 illustrate the neutral wind models for the southern hemisphere for the months of September and December 1978. The neutral winds were assumed to be independent of altitude.

2.5 Electrodynamic Drift Velocity Models

The electrodynamic drift velocity models used in the calculations were deduced by calculating values of foF2 at selected low latitude locations and adjusting the value of the drift velocity so that agreement between calculated and observed foF2 values was effected. In adjusting the electrodynamic drift velocity models, care was taken to assure that the models used were consistent with the observations of electrodynamic drift velocity at the magnetic equator reported by Woodman (1970). Different models of the drift velocity were used for different months and years. The electrodynamic drift velocity was also assumed to be independent of altitude.

2.6 Geomagnetic Field Model

A realistic geomagnetic field model was used to transform the spherical polar coordinate system r , θ , and ϕ to one describing directions parallel and perpendicular to B . The "real" field is given by Euler potentials α and β where $\vec{B} = \nabla\alpha \times \nabla\beta$ (Stern, 1965; 1967), and a full description of the technique is covered in the paper by Anderson (1973).

2.7 Solution to the Full Continuity Equation

Equation (3) was solved numerically using a Crank-Nicolson (Crank and Nicolson, 1947) implicit finite differencing scheme. The two boundaries are at 125-km altitude at the northern and southern ends of the field line. Boundary conditions for the ion density are photo-chemical equilibrium during the day and 10 ions/cm^3 at night.

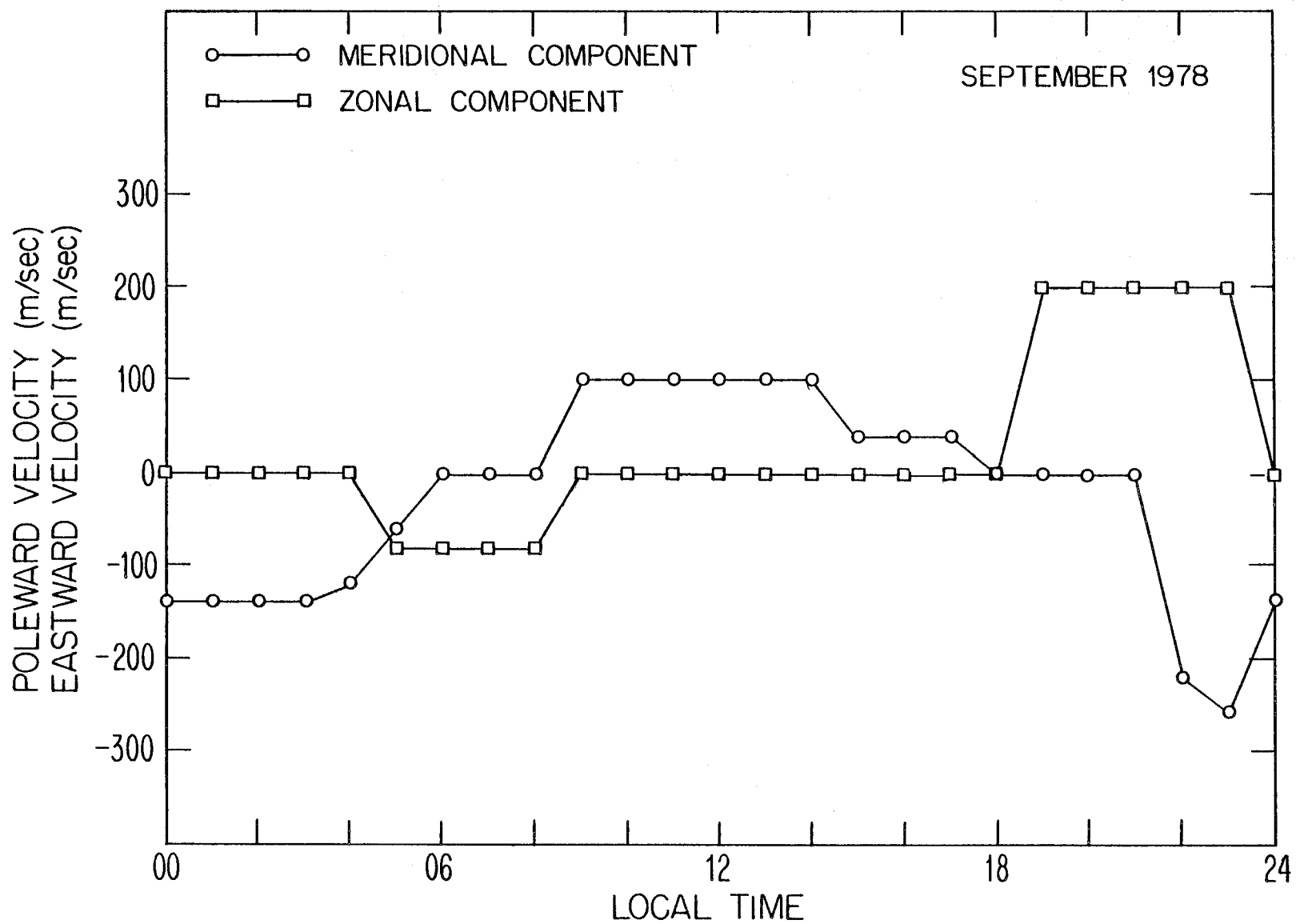


Figure 1. Meridional and zonal neutral wind model for the Southern Hemisphere for September 1978.

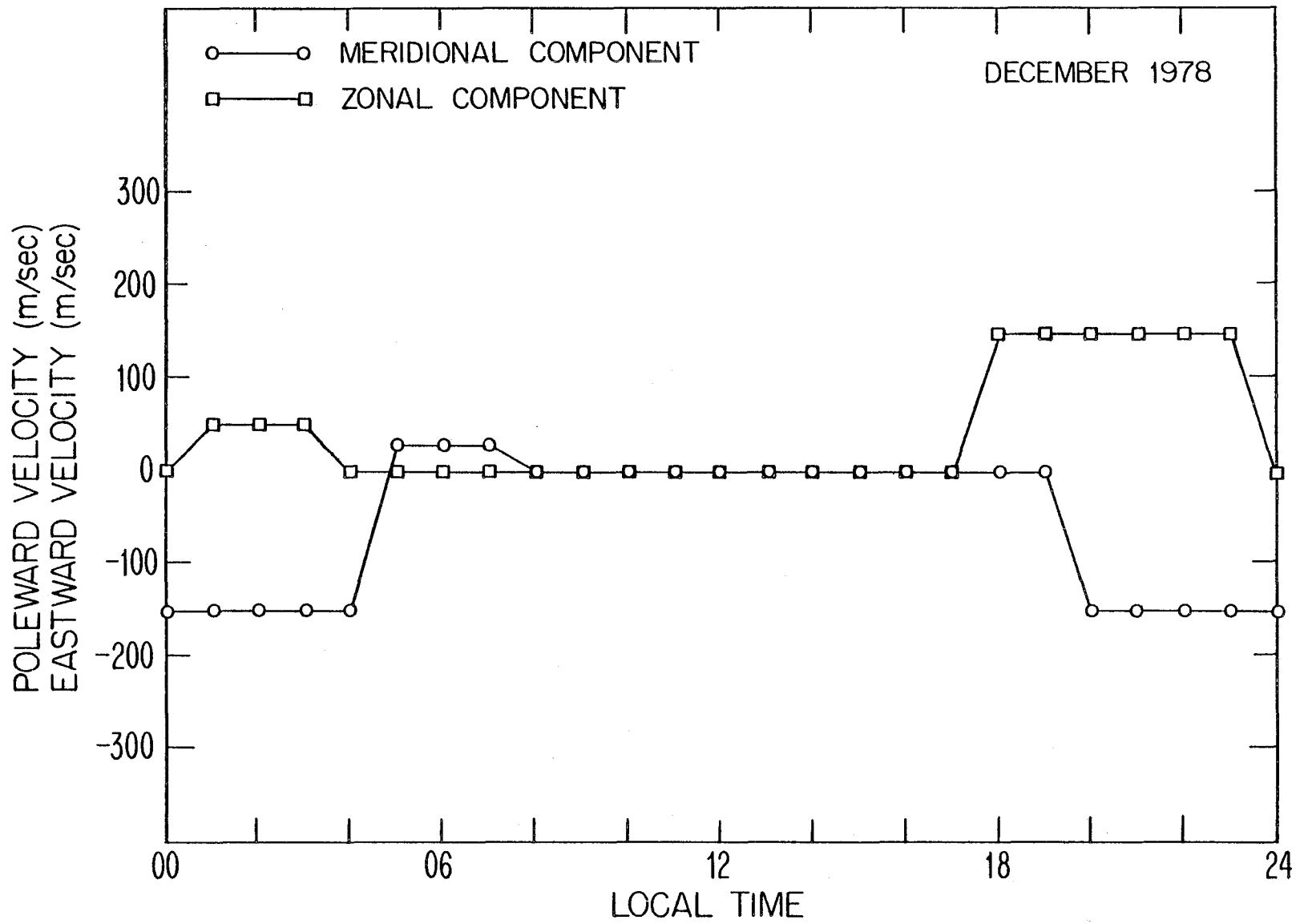


Figure 2. Meridional and zonal neutral wind model for the Southern Hemisphere for December 1978.

However, the boundary conditions are not critical, as the appropriate ion densities are reached within a few space steps. The changing size of the magnetic flux tube is taken into account in the calculations. An example of how well the theoretical calculations can be made to fit observations is given in Figure 3 which shows the results for the month of September 1978 at Auckland, New Zealand. Further discussion concerning the accuracy of the theoretical calculations will be given in later sections of the report.

The importance of using values of foF2 that are consistent with the physical processes that give rise to F region variations in developing ionospheric maps can be seen in Figure 4. The figure shows the diurnal variations of foF2 for September 1978 at three different longitudes where the declination of the magnetic field line changes but the dip angle is approximately the same. During daytime hours, the westward declination field line has the greatest peak electron density because in the Southern Hemisphere, the early morning, westward-blowing zonal wind (see Figure 1) at 80 m/sec transports ionization upward from below where the production rate is greater to higher altitudes where the loss rate is less. In geographic regions where the declination is nearly zero, the effect of the zonal wind is minimal and the results shown for -2.5° declination are obtained. Conversely, where the declination of the field line is eastward in the Southern Hemisphere, a westward-blowing neutral wind transports ionization downward into a higher loss rate region, decreasing the peak electron density such as shown for 18° declination.

During nighttime hours when the zonal wind blows eastward (1900-2400 LT), the effects of field-line declination on peak electron density are reversed. In the Southern Hemisphere an eastward blowing-wind lowers the F region if the declination is westward, thus decreasing foF2, while the same eastward wind raises the F layer where declination is eastward, causing a slower decay in foF2 with time. This can be seen by comparing the slopes of the curves shown in Figure 4 between the hours 1800 and 2200 local time.

Similar results for December 1978 are pictured in Figure 5. During the day, the peak electron density is greater for a westward declination field line, while zero and eastward declination field lines have about the same daytime peak electron density of 1×10^6 e1/cm³ (9 MHz). At night, the combination of the eastward zonal wind and equatorial meridional wind causes a reversal in the declination effects on foF2 for the same reasons given above.

It will be seen in the next section that in order to obtain a stable set of numerical coefficients that can be used to generate global maps of foF2, values of foF2 must be used in the analysis procedure at locations where observations are not

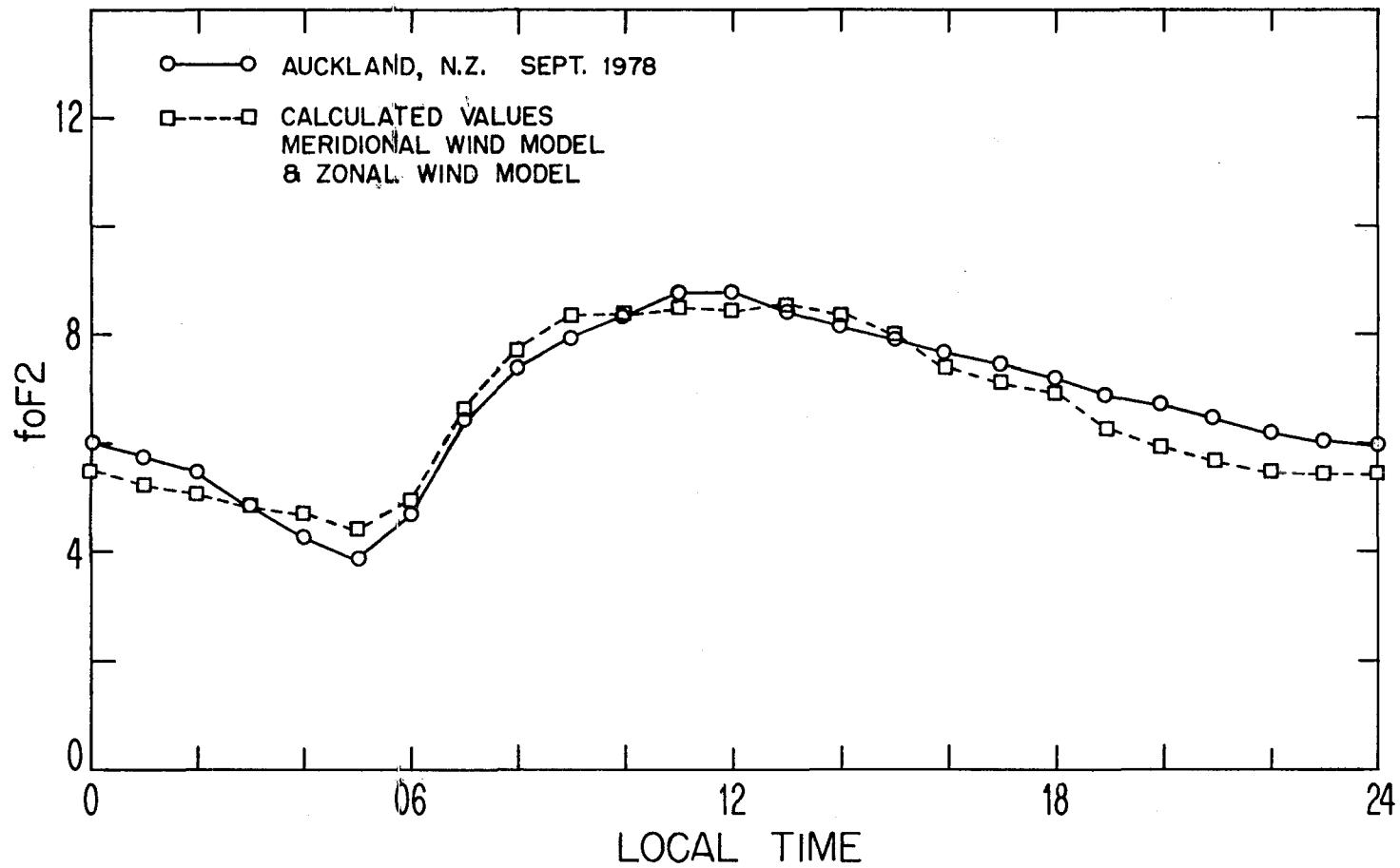


Figure 3. Comparison between median values of foF2 observed at Auckland, New Zealand, and values calculated using the theoretical model for September 1978.

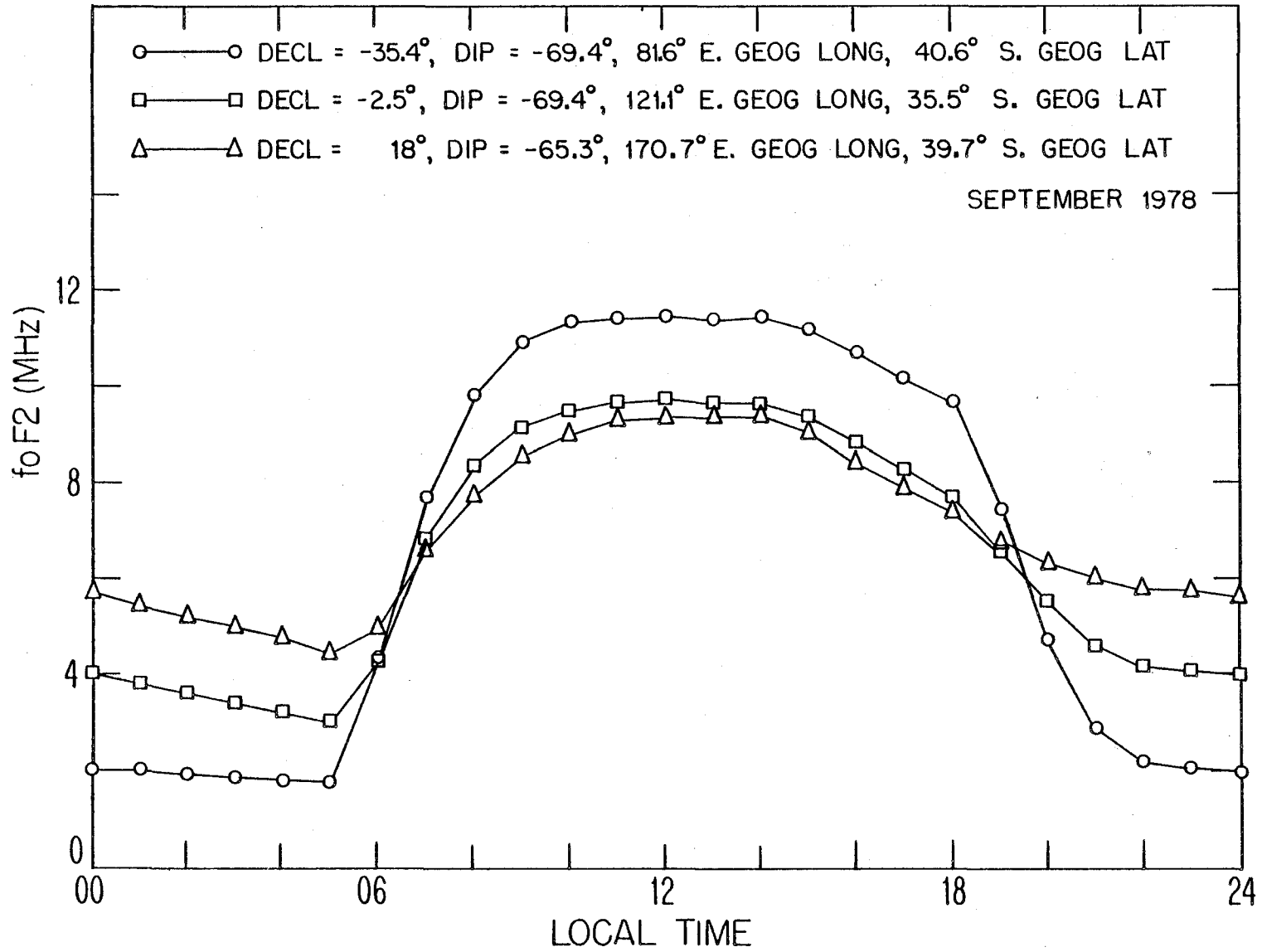


Figure 4. Diurnal behavior of foF2 during September 1978 deduced using the theoretical model with the same neutral wind model at three locations in the Southern Hemisphere having essentially the same dip but different declinations.

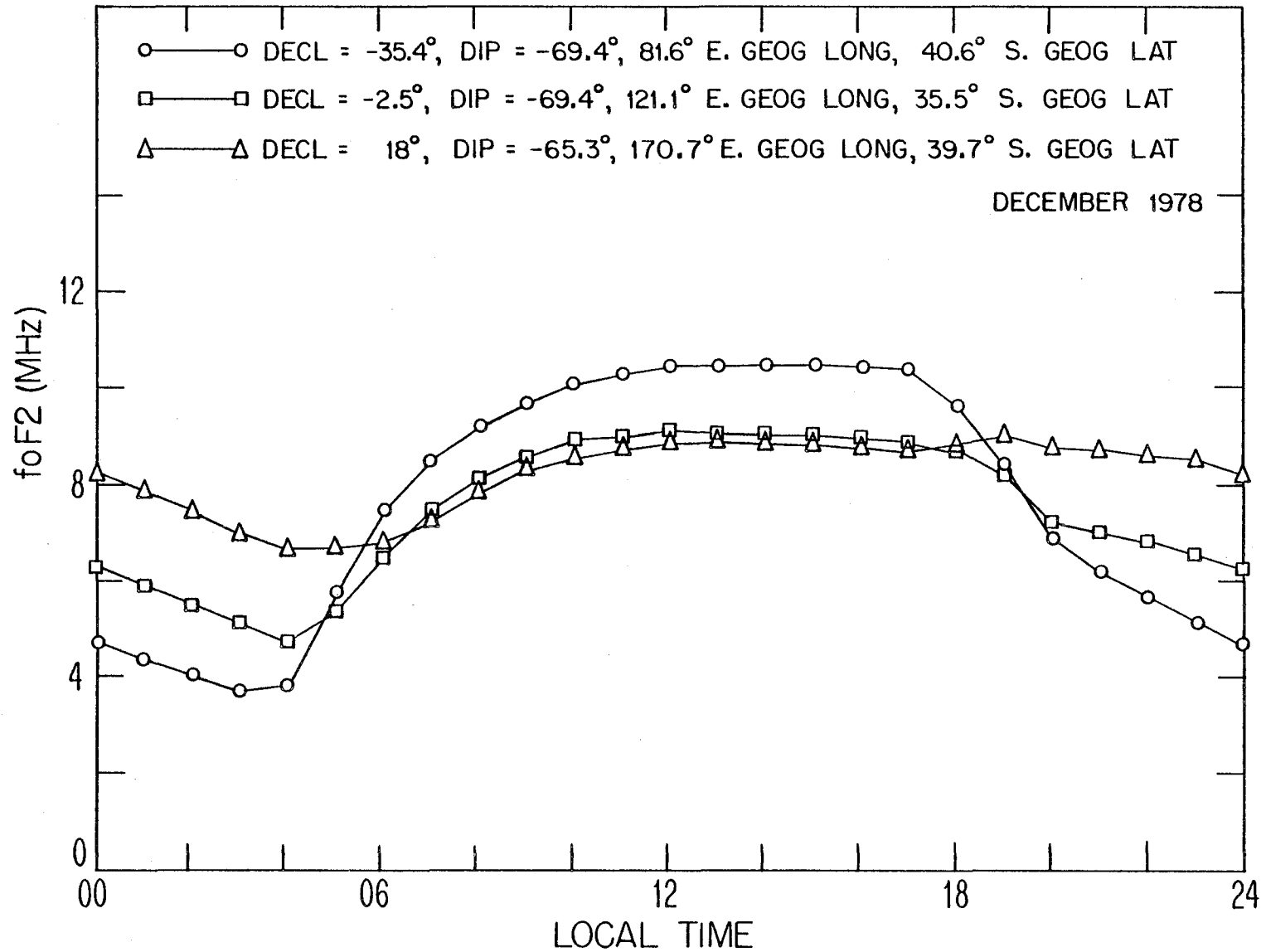


Figure 5. Diurnal behavior of foF2 during December 1978 deduced using the theoretical model with the same neutral wind model at three locations in the Southern Hemisphere having essentially the same dip but different declinations.

available. Thus it is necessary to extrapolate observations of foF2 into regions of the globe where data are not available. In previous studies (Jones et al., 1969; Jones and Obitts, 1970) this extrapolation was undertaken simply by moving available data to inaccessible regions and adjusting for time differences. The results shown in Figures 4 and 5 demonstrate the importance of accounting for the effects of the magnetic declination in specifying foF2. The theoretical model provides a convenient and valid method to obtain physically realistic values of foF2 at locations that are generally inaccessible to routine observation.

3. METHOD OF ANALYSIS

3.1 Mathematical Basis

In order to generate global maps of the F2 region critical frequency using observed as well as theoretical data, it is necessary to determine the appropriate functional form needed to represent the important variations in the data. These variations are for the most part tied to the large-scale temporal and spatial variations of the ionosphere. Because of specific applications of the final results, it is necessary that the functions chosen allow the use of digital computers for evaluation and prediction. Consideration must be given to the nature of the original data itself, for example:

1. that the data are 3 dimensional (time, geographic latitude, geographic longitude) and a simple set of functions will not represent the variations;
2. that the data have certain amounts of noise or random fluctuations that can cause difficulty in deciding how many functions to use in the representation;
3. and that geographic distribution of the data presents problems in fitting the data and preserving the stability of the final result in areas where few data points (or observing data) are available (ideally equally spaced data distributed uniformly over the globe and in time is desired).

The usual method of representing global variations of geophysical data is to utilize spherical harmonic analysis. This approach provides functions that are periodic in longitude and constant at the poles. The classical surface spherical harmonics which satisfy Laplace's equations, however, are not orthogonal with respect to the positions of ionospheric data available in this study. Therefore, two sets of functions were chosen. A set of orthogonal polynomials was chosen to represent geographic variations. The diurnal variations then need only be represented by a periodic function, and a Fourier series was chosen to provide this representation.

3.1.1 Diurnal analysis

The most natural method for representing the diurnal variation of foF2 is to employ a Fourier representation as ionospheric characteristics are periodic functions of time. Moreover, the trigonometric functions associated with Fourier analysis are automatically orthogonal with respect to equally spaced data points. Advantages of using Fourier series are that adjusting the data for differences in recording times is greatly simplified, the noise inherent in the observations is more easily separated from the true diurnal variation, and the resultant accuracy of the Fourier fit to the data can be readily assessed using least squares techniques.

The application of Fourier analysis to periodic data sets may be found in texts on numerical analysis. For the particular application at hand let $f(x)$ be a periodic function of period 2π whose values are measured at N equally spaced points. Then

$$x_i = \frac{2\pi i}{N}, \quad i = 0, 1, \dots, N.$$

Let these values be denoted by the following y_0, y_1, \dots, y_{11} where $y_0 = y_N$. A Fourier analysis of these data using k harmonics ($2k + 1 \leq N$) yields an expression of the form

$$Y_k(x) = a_0 + \sum_{j=1}^k [a_j \cos jx + b_j \sin jx] \quad (4)$$

where
$$a_0 = \frac{1}{N} \sum_{i=1}^N y_i$$

$$a_j = \frac{2}{N} \sum_{i=1}^N y_i \cos jx_i \quad (5)$$

$$b_j = \frac{2}{N} \sum_{i=1}^N y_i \sin jx_i$$

for all values of k where ($2k + 1 \leq N$). The value of $Y_k(x)$ is a best approximation in the sense of least squares. Cast in another manner, the equation

$$R_k^2 = \frac{1}{N} \sum_{i=1}^N [y_i - Y_k(x_i)]^2 \quad (6)$$

is a minimum with respect to all real valued coefficients a_j, b_j . Therefore, R_k can be used as a measure of goodness of the approximation. In the current application the 24 hourly measurements of foF2 are available usually in local standard time and therefore must be translated to local time. It has been established (Jones and Gallet, 1962) that eight harmonics in the Fourier analysis is an optimum number of harmonics to smooth out noise and at the same time give a good representation of the diurnal variation of foF2. After fitting the diurnal data with the Fourier series, the Fourier coefficients are shifted in time so that the data at each station can be represented in local time. The Fourier coefficients representing the diurnal variation of the foF2 data are then fit with respect to the geographic location at which the data were taken.

3.1.2 Geographic analysis

The set of functions chosen to represent the geographic variation of the Fourier coefficients are given in Table 2.

This set of geographic functions $G_k(\lambda, \theta)$ given in Table 2 are analogous in some respect to spherical harmonics. The main latitudinal variation terms correspond to zonal harmonics, and the mixed latitudinal and longitudinal terms involving $\cos \theta$ or $\sin \theta$ (along with the terms involving $\cos 2\theta$ and $\sin 2\theta$) correspond to the tesseral harmonics of the first and second order, respectively. The series of functions, $G_k(\lambda, \theta)$, have many desirable properties of a spherical harmonic analysis. They are periodic in longitude; they are constant at the poles; and they are weighted according to latitude by the functions $\cos \lambda, \cos^2 \lambda, \dots$. Thus as the corresponding zonal and tesseral harmonics are merely linear combinations of the functions $G_k(\lambda, \theta)$ and are fitted by the same criterion, that of mean least squares, the resulting approximations are the same as would be obtained from spherical harmonic analysis.

In formulating the geographic analysis, let $f(x)$ be a function whose values y_1, y_2, \dots, y_N are measured at an arbitrary given set of points x_1, x_2, \dots, x_N . Then if k is an integer such that $0 \leq k < N$, the problem is that of determining the polynomial

Table 2: Set of functions chosen to represent the geographic variation of the Fourier coefficients

k	$G_k(\lambda, \theta)$
0	1
1	$\sin\lambda$
2	$\sin^2\lambda$
\vdots	\vdots
p_1	$\sin^{p_1}\lambda$
$p_1 + 1$	$\cos\lambda \cos\theta$
$p_1 + 2$	$\cos\lambda \sin\theta$
$p_1 + 3$	$\sin\lambda \cos\lambda \cos\theta$
$p_1 + 4$	$\sin\lambda \cos\lambda \sin\theta$
\vdots	\vdots
$p_2 - 1$	$\sin^a\lambda \cos\lambda \cos\theta$
p_2	$\sin^a\lambda \cos\lambda \sin\theta$
$p_2 + 1$	$\cos^2\lambda \cos 2\theta$
$p_2 + 2$	$\cos^2\lambda \sin 2\theta$
$p_2 + 3$	$\sin\lambda \cos^2\lambda \cos 2\theta$
$p_2 + 4$	$\sin\lambda \cos^2\lambda \sin 2\theta$
\vdots	\vdots
$p_3 - 1$	$\sin^b\lambda \cos^2\lambda \cos 2\theta$
p_3	$\sin^b\lambda \cos^2\lambda \sin 2\theta$
\vdots	\vdots

$$a = \frac{p_2 - p_1}{2} - 1$$

$$b = \frac{p_3 - p_2}{2} - 1$$

where λ = Geographic latitude

θ = Geographic longitude

$$Y_k(x) = D_0^k + D_1^k x + \dots + D_k^k x^k \quad (7)$$

of degree k for which the sum of squares of residuals

$$E_k = \sum_{i=1}^N [y_i - Y_k(x_i)]^2$$

has a minimum value with respect to all real values coefficients D_j^k can be determined. In terms of orthogonal polynomials, the desired function may be written very simply as

$$Y_k(x) = d_0 P_0(x) + d_1 P_1(x) + \dots + d_k P_k(x) \quad (8)$$

where the coefficients in the orthogonal system are

$$d_j = \left[\sum_{i=1}^N y_i P_j(x_i) \right] / C_j \quad (9)$$

The numbers C_j are given by

$$C_j = \sum_{i=1}^N [P_j(x_i)]^2 \quad (10)$$

The coefficients in the orthonormal system are

$$D_j = d_j \sqrt{C_j} \quad (11)$$

The sum of squares of residuals E_k in the orthonormal system may then be obtained from

$$E_k = \sum_{i=1}^N y_i^2 - D_0^2 - D_1^2 - \dots - D_k^2$$

and the root-mean-squared (RMS) error e_k from

$$e_k = E_k / [N - (k + 1)] \quad (12)$$

The computational problems in the orthogonal system are greatly simplified as the normal equations which must be solved are reduced to a trivial system, and the danger of large roundoff errors resulting from matrix inversion is reduced. Each term $d_j P_j(x)$ in the series (8) is independent of other terms. As a consequence, the degree of the approximating polynomial may be increased without affecting the terms already obtained and, in some cases, tests for statistical significance may be applied to each term.

The determination of the best degree of the approximating polynomials can not be generalized. Methods from regression theory may be used when the observed data satisfy certain statistical assumptions. For example, if the observed data are independent and normally distributed about a theoretical regression with a common standard deviation, a Student's T test may be applied to determine the significance of the terms $d_j P_j(x)$.

An application of this test is commonly made using the numbers e_k^2 defined in Equation (12). As long as these numbers decrease significantly as k increases, the approximations are considered to be improving. However, when the e_k^2 cease to diminish, the series should be cut and the degree k thus defined.

Graphical methods can also be used to determine a "best" value for the degree k . For example, a series of graphs of the functions $Y_k(x)$ for $k = 1, 2, \dots$ compared with a plot of the data y_i will show quite often that as k increases the graphs will tend to "converge" to a fixed curve around a certain value of k , but for higher k values the graphs begin to oscillate wildly between data points. Thus in some sense an "asymptotic" solution may be obtained for the "best" degree k .

3.2 Data Used in Constructing Maps

In developing numerical maps of ionospheric data, it is necessary to insure that data exist at sufficient locations so that the mapped values of foF2 do not have negative values. Early attempts by Jones and Gallet (1962) showed that using a set of functions that would adequately represent the measured ionospheric data could lead to instabilities in the maps in areas where the data were either non-existent or sparse.

In order to solve this problem, it is necessary to somehow use all ionospheric measurements regardless of when they were made. For example, the attempt to numerically represent ionospheric data was not feasible until the International

Geophysical Year (July 1957 - December 1958) when the number of operating vertical-incidence ionosphere stations almost tripled. Ionospheric data were available for the 19th cycle of solar maximum for approximately 150 ionosphere stations. In order to obtain comparable data for solar minimum, the initial work of Jones and Gallet (1962) provided for the interpolation or "prediction" of median values of foF2 for the 1954 solar minimum from measurements which were available after the IGY period. In other cases, the predictions may have been based on measurements made prior to the given year. Predictions were made for each hour from the correlation of available data with a solar index. The method of prediction is well-known and widely used (Crow and Zacharisen, 1960). It consists of polynomial interpolation (first or second degree) of the characteristic on an appropriate solar index such as running average sunspot number. Predictions of this type are referred to as "B-data," whereas ionospheric measurements and their medians are designated as "A-data." Predicted data obtained in a similar manner have been applied in meteorology by using a forecast where no data are available (see, for example, the work of Bergthorsson and Doos [1955]). Such "data" have also been employed in geomagnetism when the secular variation is used to predict the value of a magnetic component for a given epoch (Vestine et al., 1947).

The B-data helped to control instability in the ionospheric maps, particularly in the polar regions where stations were not available prior to the IGY. However, a number of critical areas still existed, and in order to control the instabilities in these areas, a "screen" analysis was performed. For this analysis, it was assumed that, as the main geographic variation was the magnetic dip latitude (inclination), this would provide the best first approximation of ionospheric data. Basically, the effect of the screen analysis was to extrapolate values of foF2 observed in land regions to ocean areas without introducing further instabilities by including higher order longitude terms. The screen analysis served the purpose of providing reasonable representations (called "C" data) in the ocean areas, but was never considered to be an accurate or even adequate representation for the ocean areas. Using the theoretical model to provide data for these areas instead of the original "screen" analysis introduces physical consistency into the maps.

4. RESULTS OF THE GLOBAL REPRESENTATIONS OF foF2 USING THE THEORETICAL foF2 VALUES

To determine the usefulness of employing theoretically derived foF2 values with the world-wide observations of foF2, the maps for the months of July, September, and December for a year of low (1975) and high (1978) solar activity were selected for study. The number of vertical-incidence ionosphere stations has been steadily decreasing since the IQSY (1964), and as a result, the number of "A" data points (actual observations) used in generating the maps was less than 90 for 1975 and less than 80 for 1978. This required updating and revising the regression analyses for a large number of "B" stations (predicted data). For the mid-latitude analysis, "screen points" or "D" data were generated from the theoretical model for L values of 1.25, 1.5, 1.75, 2.0, 2.5, 3.0, and 4.0 at approximately every 15° longitude (126 "D" points were available for each hemisphere). As the hypothesis was to improve the representations in areas where no "A" or "B" were available, a large number of "D" points were eliminated. In the final analysis, 63 "D" points were used in the Southern hemisphere and only 45 "D" points were used in the Northern hemisphere. A typical distribution of "A", "B", and "D" data points is shown in Figure 6 for December 1975. The shaded area in this map indicates the low latitude area. The theoretically derived data points for low latitudes are not included in the results presented in this report. The unshaded area between the two heavier lines in each hemisphere indicates the area for which "D" (or theoretically derived) data points were included. The number on the figure next to selected "D" data points in the Southern Hemisphere refers to locations which will be used in subsequent discussions.

For the new analysis using theoretical data, no attempt would be made to test any new functions for representing either the diurnal or geographical variations. Therefore, the same number of Fourier harmonics were used to represent the diurnal variation, and the same number of degrees for the zonal and tesseral harmonics were used to represent the geographical variations as had been used in the previous global representations. Some change was made in the order of the computation, but this had little effect in the middle latitude regions. The "screen" analysis described in section 3.2 was completely omitted from the results presented here. For the 1954 to 1958 analyses, 230 data points (A, B, and C) were used. For 1975, and 1978, only 190 and 180 A, B, and D data points have been used.

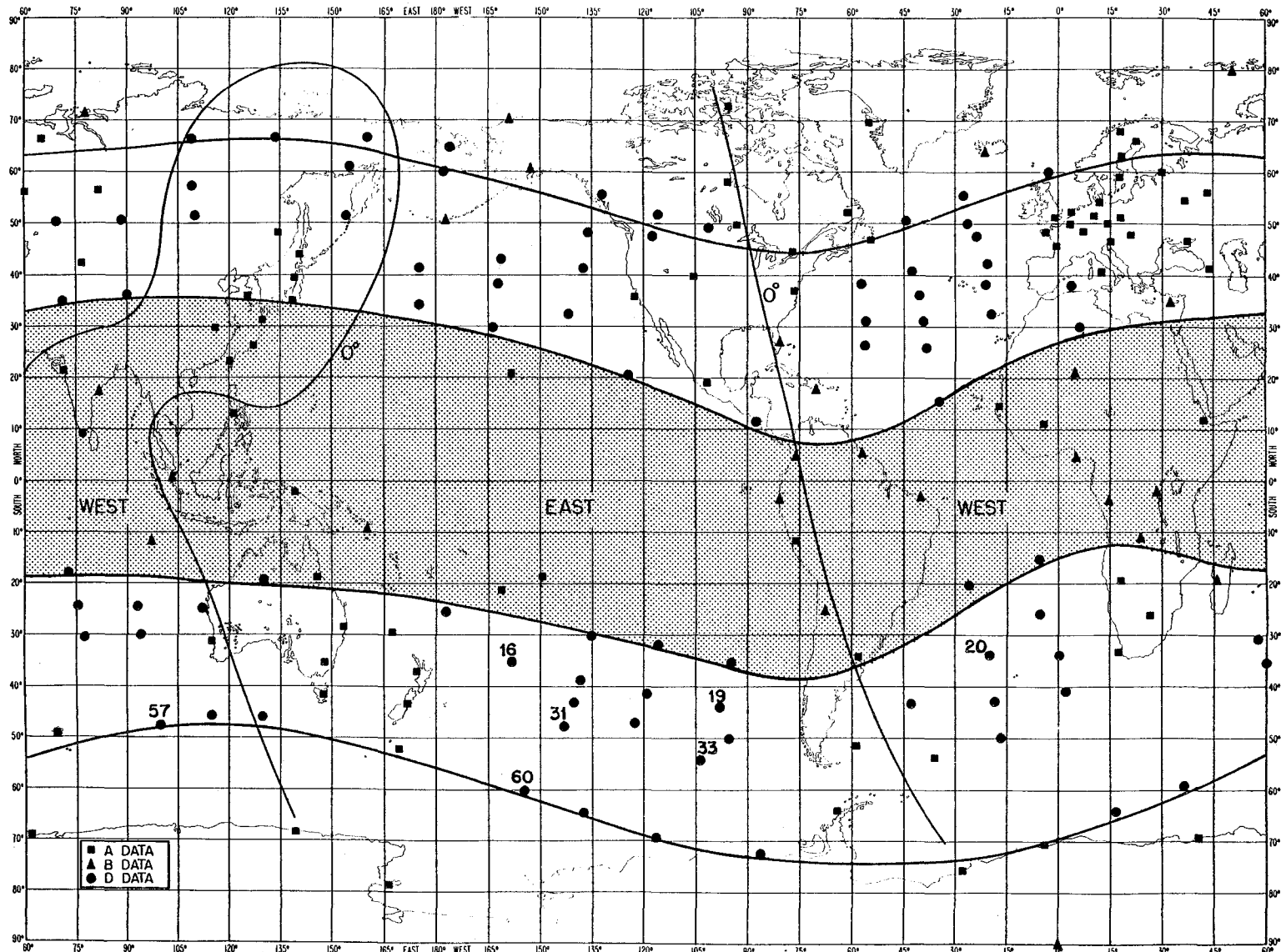


Figure 6. Global distribution of data points used to generate maps of foF2 for December 1975. The two heavy lines shown on the Figure are the locations of the 0° declination.

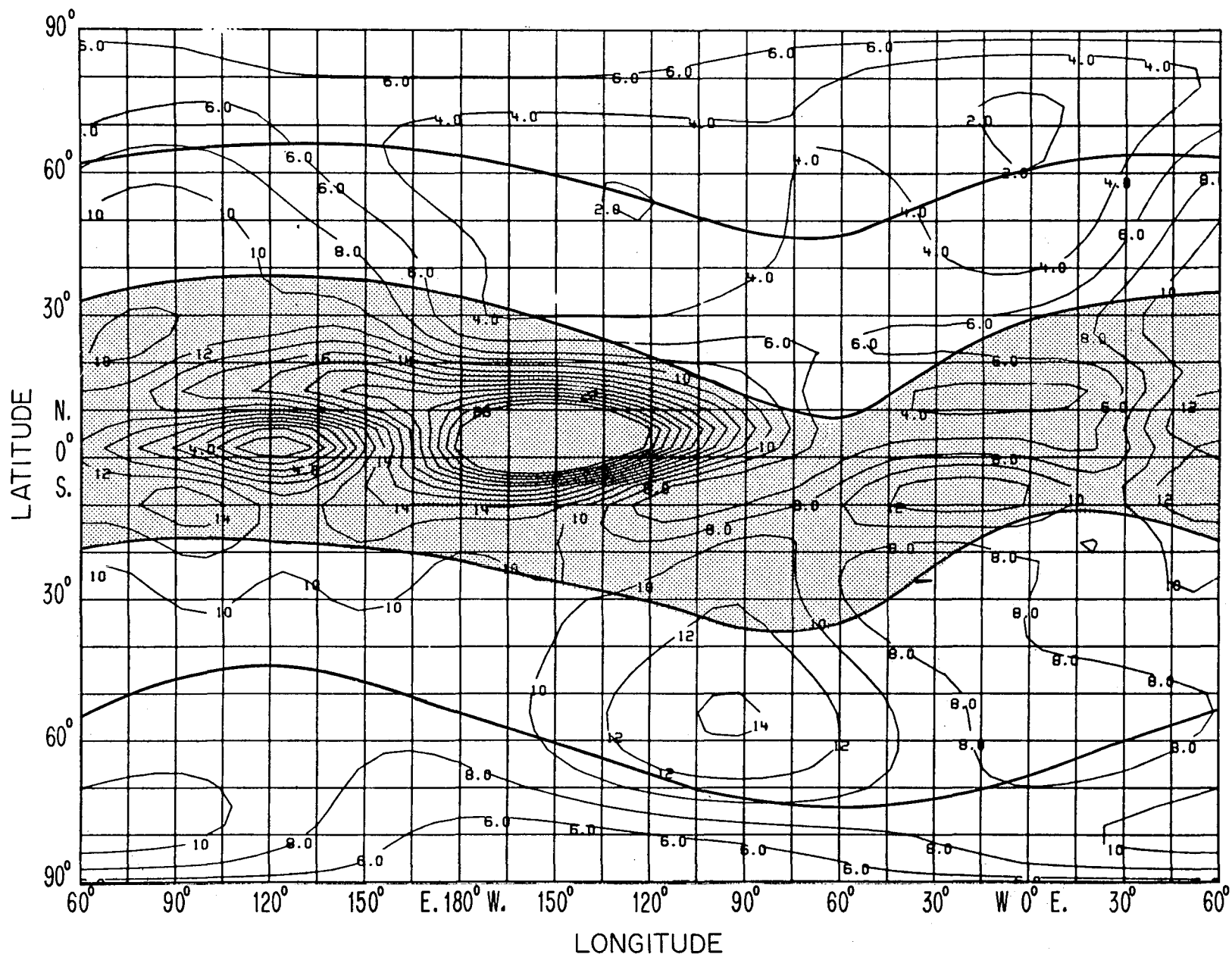


Figure 7. Contour map of the global representation of the median value of foF2 for December 1975 at 06 UT.

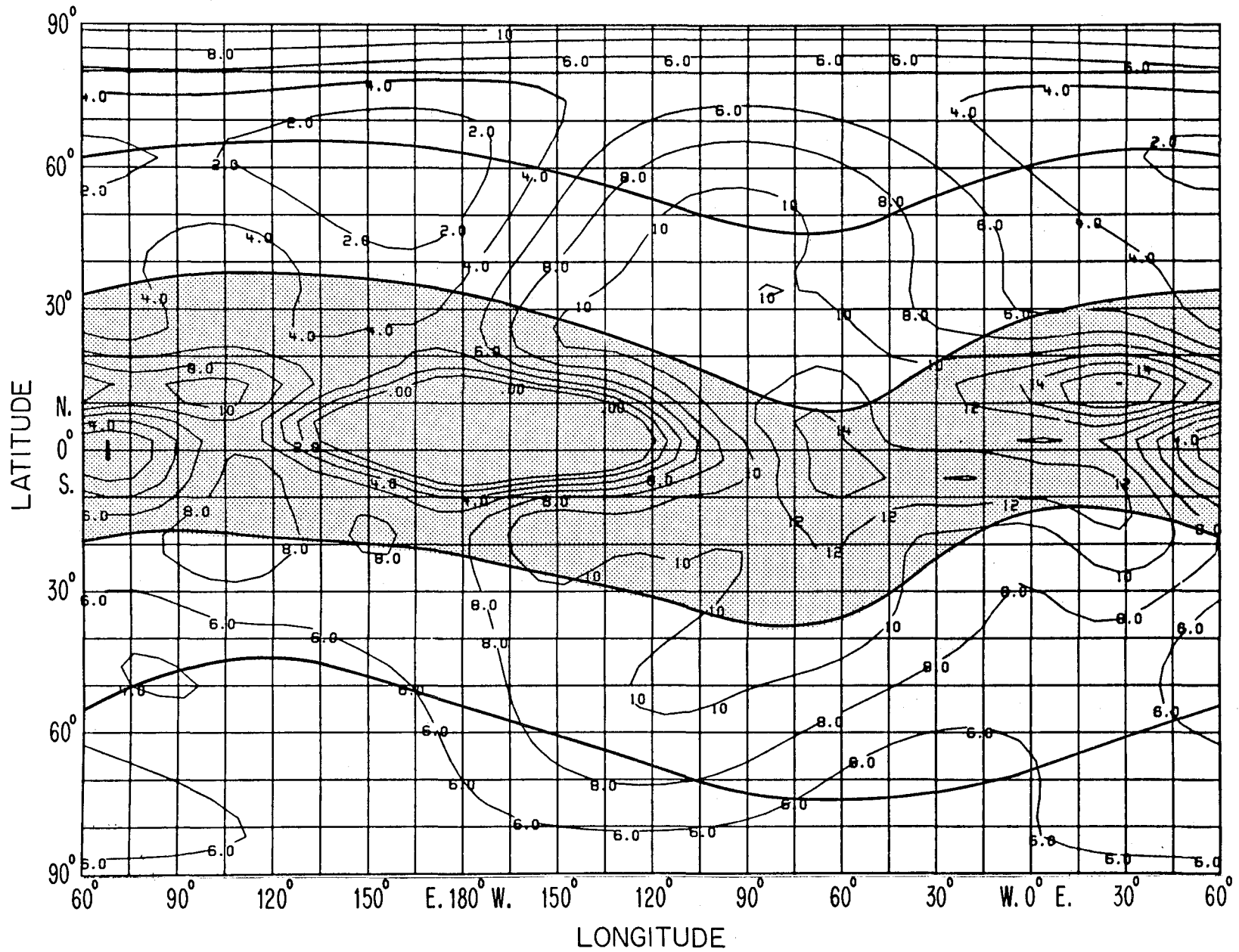


Figure 8. Contour map of the global representation of the median value of foF2 for December 1975 at 18 UT.

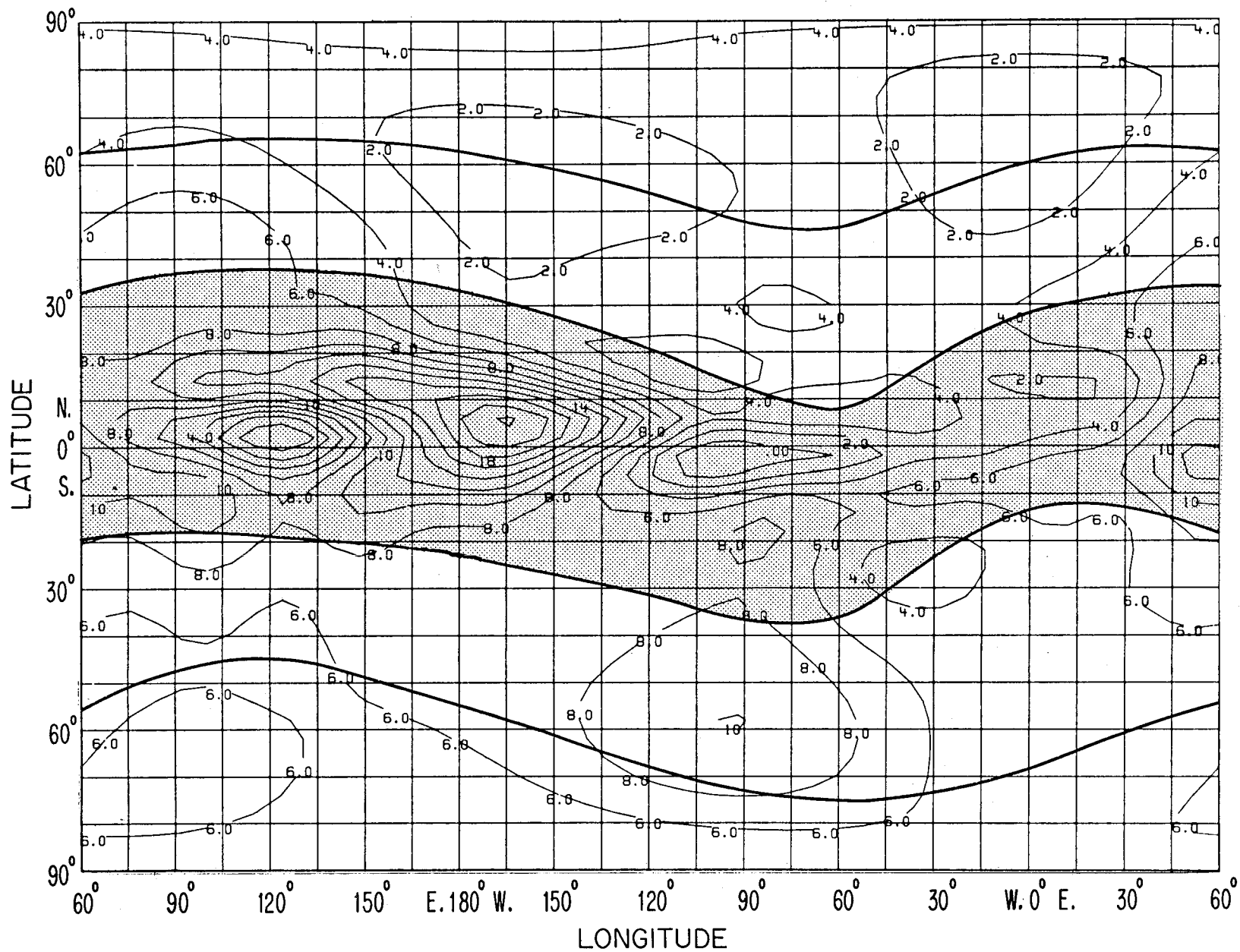


Figure 9. Contour map of the global representation of the median value of foF2 for December 1978 at 06 UT.

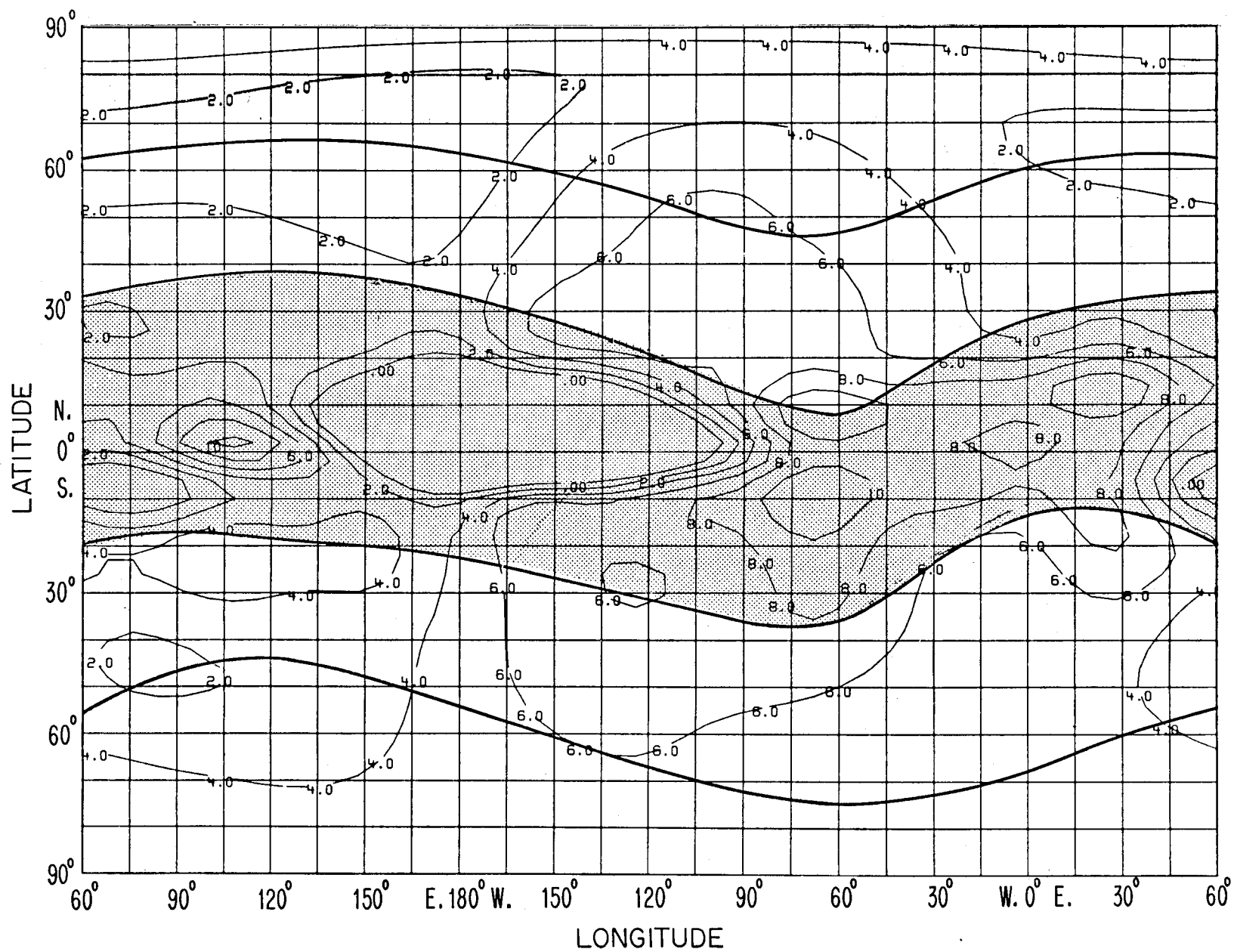


Figure 10. Contour map of the global representation of the median value of foF2 for December 1978 at 18 UT.

Sample contour maps of the global representation of foF2 for 06 and 18 UT for December 1975 and 1978 are presented in Figures 7, 8, 9, and 10. The contours at low latitudes (shaded areas) in the Pacific Ocean illustrate the magnitude of the instabilities resulting from an inadequate distribution of data points in the analysis procedure. In particular, the area within the zero contour is negative due to a lack of A, B, or D points in generating the coefficients for Figures 7, 8, 9, and 10 in the Pacific Ocean. Because the previous global representations were less reliable for the southern hemisphere than for the northern hemisphere, the emphasis in this work was placed on the results for the southern hemisphere.

In order to gain some estimate of the amount of improvement afforded by incorporating the theoretical foF2 values into a global mapping scheme, it is necessary to compare the theoretical values of foF2 with those determined from the existing coefficients and with actual observations. It is not possible, in general, to obtain a large number of observations of foF2 in the southern hemisphere. There are however observations of foF2 for the southern hemisphere that have been obtained from the ISS-b satellite. Matuura (1979) has deduced global maps of foF2 from the ISS-b satellite observations averaged over the months August to December 1978. These maps provide a means to assess the improvement in foF2 in an indirect manner.

Figure 11 shows three longitudinal distributions of foF2 at three latitudes (30°S, 40°S, and 50°S) for December 1978, 1000 UT. Shown is the distribution deduced by incorporating theoretical values of foF2 into the mapping scheme, and the distribution of foF2 resulting from the CCIR numerical coefficients. Also indicated on the figure are values of foF2 deduced from the data collected by the ISS-b satellite. Only data collected in September 1978 are shown in the figure. While differences between observed and mapped values of foF2 exist, the values of foF2 deduced using the theoretical model represent the observations better than do the values determined from the CCIR coefficients alone.

Figure 12 shows a comparison between the diurnal variation of foF2 deduced from the theoretical calculations (depicted as a dashed line) and the diurnal variation of foF2 deduced from the CCIR coefficients (solid line). The diurnal variation of foF2 in this case was determined for September 1978 at the location closest to Kerguelen (49.4°S and 70.3°E geographic). In addition to the values of foF2 calculated by the theoretical model and by the CCIR coefficients, the median values of foF2 observed at Kerguelen during September 1978 are shown in Figure 12. Also indicated on the figure are values of foF2 deduced from the data collected by the ISS-b satellite. The theoretical model yields results that agree much

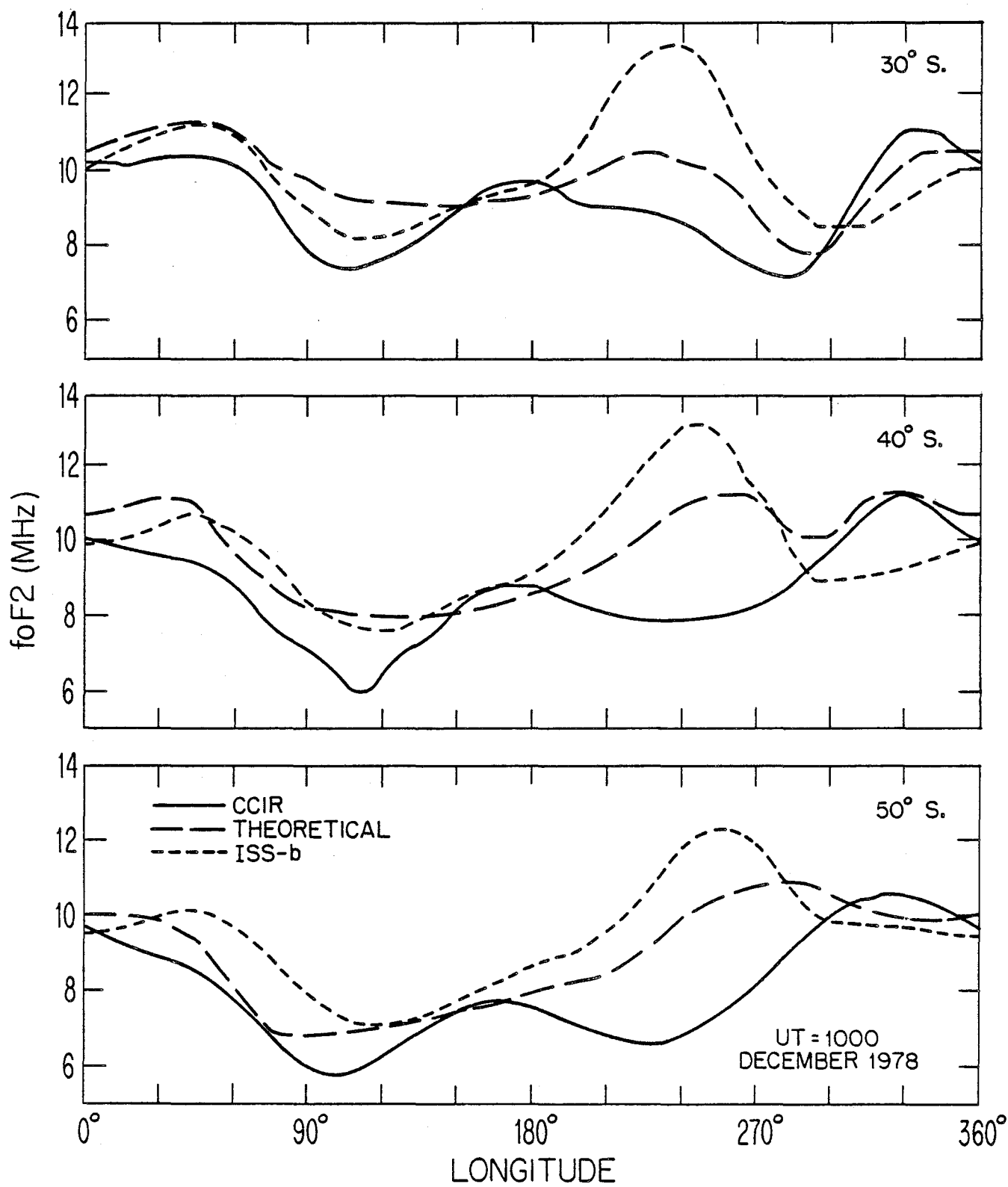


Figure 11. Longitudinal distribution of foF2 at 30°, 40°, and 50° south latitude for December 1978 at 10 UT.

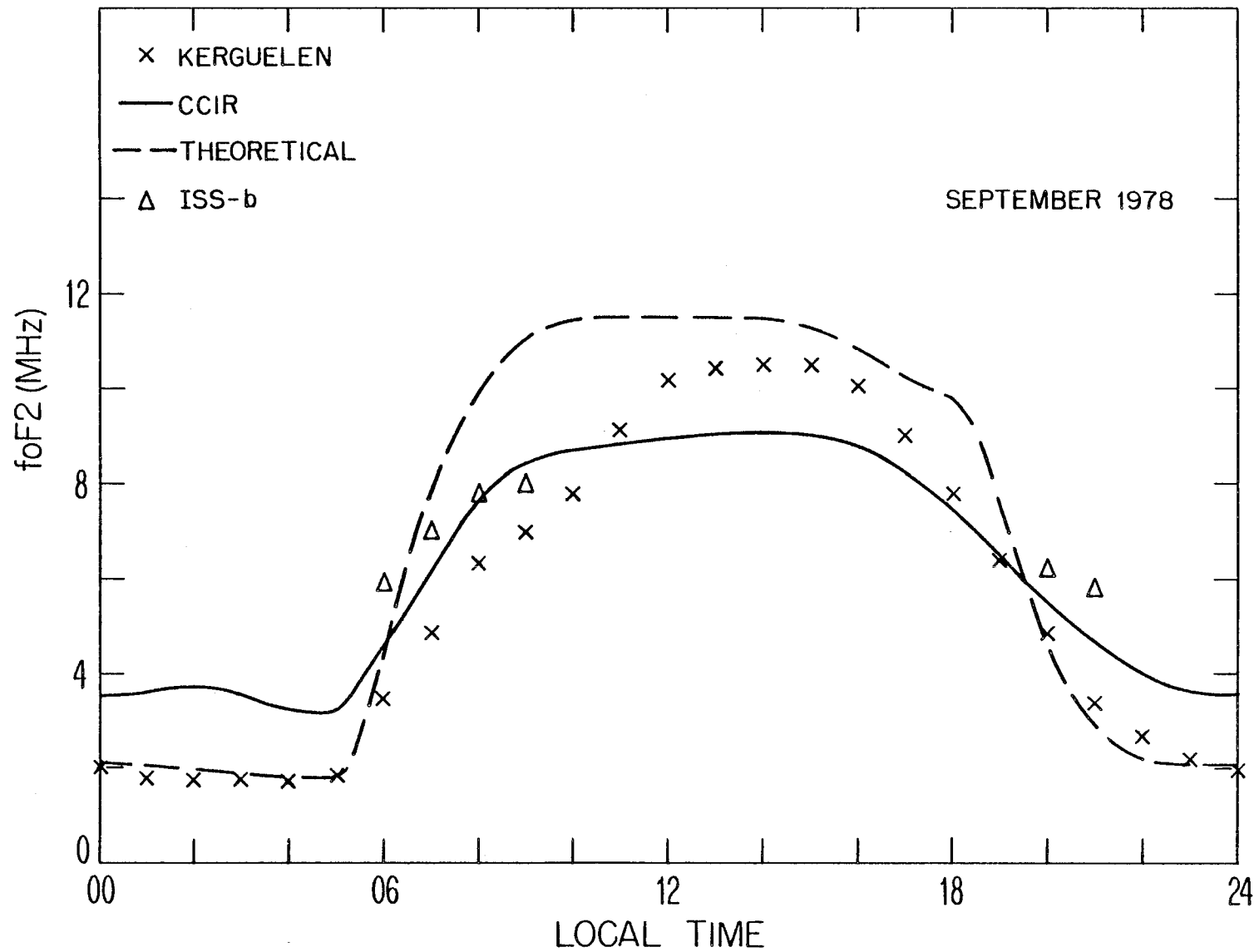


Figure 12. Comparison between the diurnal variation of foF2 observed at Kerguelen during September 1978 with that deduced from the theoretical calculations and the CCIR coefficients.

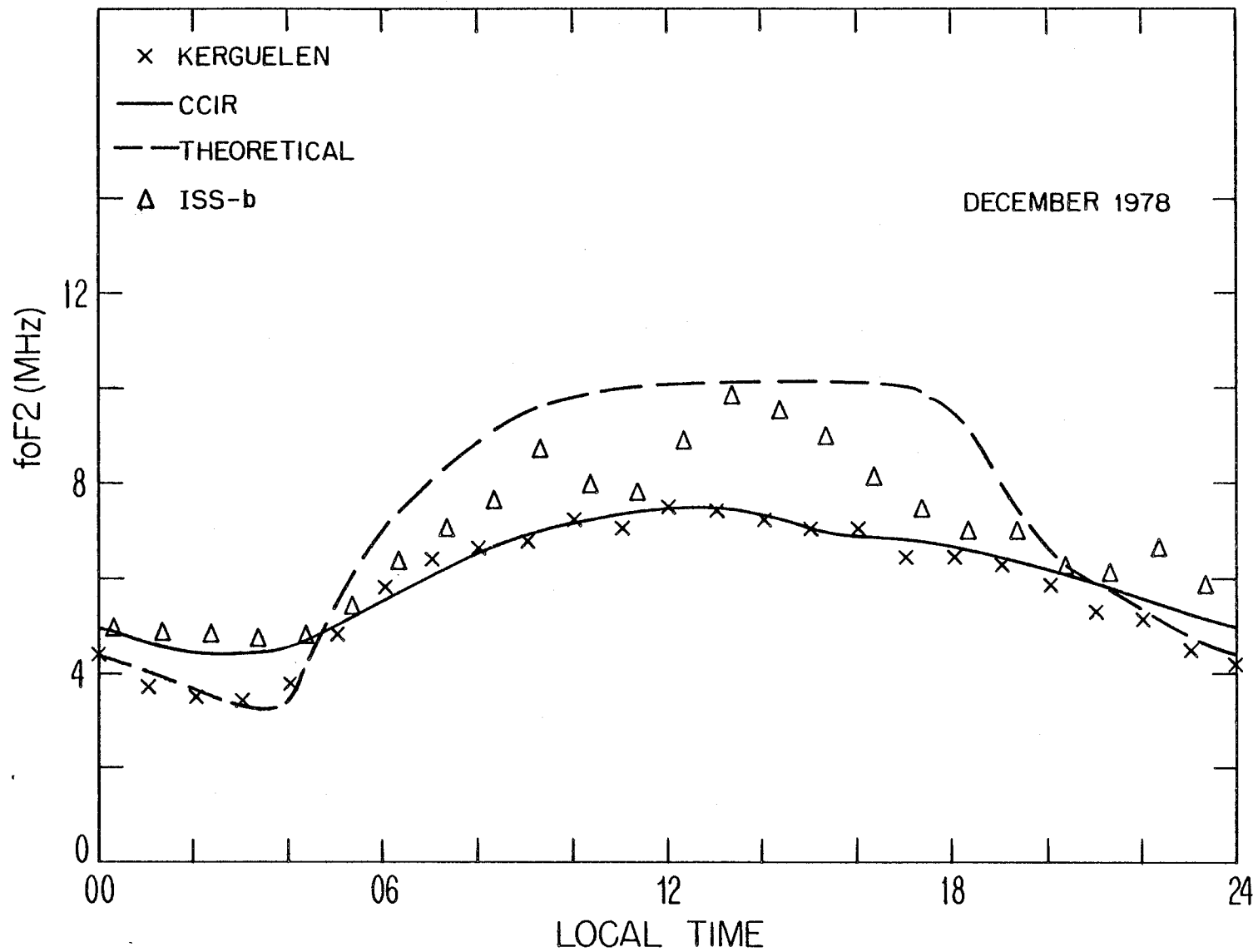


Figure 13. Comparison between the diurnal variation of foF2 observed at Kerguelen during December 1978 with that deduced from the theoretical calculations and the CCIR coefficients.

better with the observations, particularly at night, than results obtained from the CCIR coefficients.

Figure 13 provides a similar comparison for December 1978. In this example, it is seen that improvement afforded by use of the theoretical model is not as straight-forward as seen in Figure 12. The theoretical model provides a better estimate of the nighttime values of foF2 observed at Kerguelen than do the CCIR coefficients. The CCIR coefficients, on the other hand, provide a better representation for the daytime values of foF2 observed at Kerguelen. The theoretical model, however, appears to provide a better estimate of the daytime values of foF2 observed by the ISS-b satellite during December 1978.

Figures 14, 15, and 17 show a comparison between the observed or theoretical foF2 values with the representations derived from maps resulting from the new analyses (designated new representation) and the values predicted from the CCIR coefficients (1978a). The set of "A" stations and "D" points illustrated in each figure are located at approximately the same modified dip latitude, and the exact locations are given in Table 3. The purpose of the figures is to demonstrate that use of the values of foF2 derived from the theoretical model has improved the mapped representation in the ocean areas while preserving the accuracy of the A stations in the existing CCIR representation.

In Figure 14, the improvement of the theoretical foF2 over the existing CCIR values is seen for December 1978. The new representations for Brisbane, Norfolk Island, and Falkland Island are equally as good as that obtained from the CCIR coefficients. However, for 1975 the new analysis is significantly better as the CCIR coefficients appear to predict substantially higher foF2 values in the daytime. The same effect is observed at the locations indicated as 16, 19, and 20 in the daylight hours. However, the most interesting change is noticeable in the comparison for the night-time hours for the "D" points, particularly in December 1978. The theoretical points 16 and 19 indicate higher foF2 values for the South Pacific area, but the theoretical point 20, in the South Atlantic, indicates that the foF2 at night is much lower than the CCIR predictions for 1975 and 1978. Both of these results are consistent with reported comparisons between satellite observations and the CCIR coefficients. It should be noted that the new representation for Falkland Island, which is located between points 19 and 20, is as accurate as the old representation for December 1978 and somewhat better for December 1975.

In the second set of comparisons, Figure 15, the first station shown is Mundaring. The data from this station were used to establish the parameters for the theoretical model for the Southern Hemisphere. For the four stations shown in

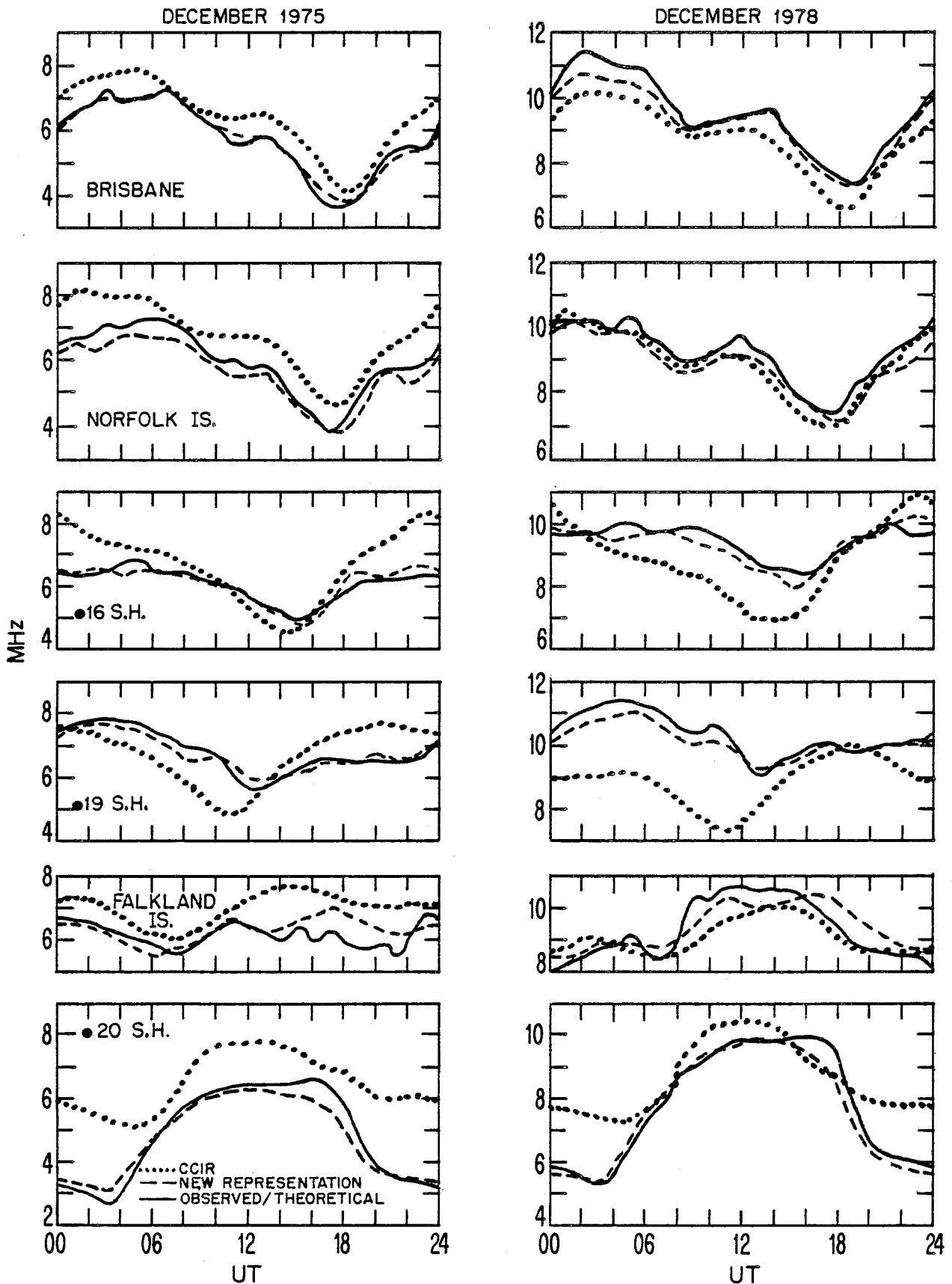


Figure 14. Comparison between the diurnal variation of foF2 for December 1975 and December 1978 deduced from the existing CCIR coefficients, the new coefficients developed in this study, and from the theoretical model or from observations where available. Plots are shown for observations at Brisbane, Norfolk Island, and Falkland Island and theoretical calculations at points 16, 19, and 20.

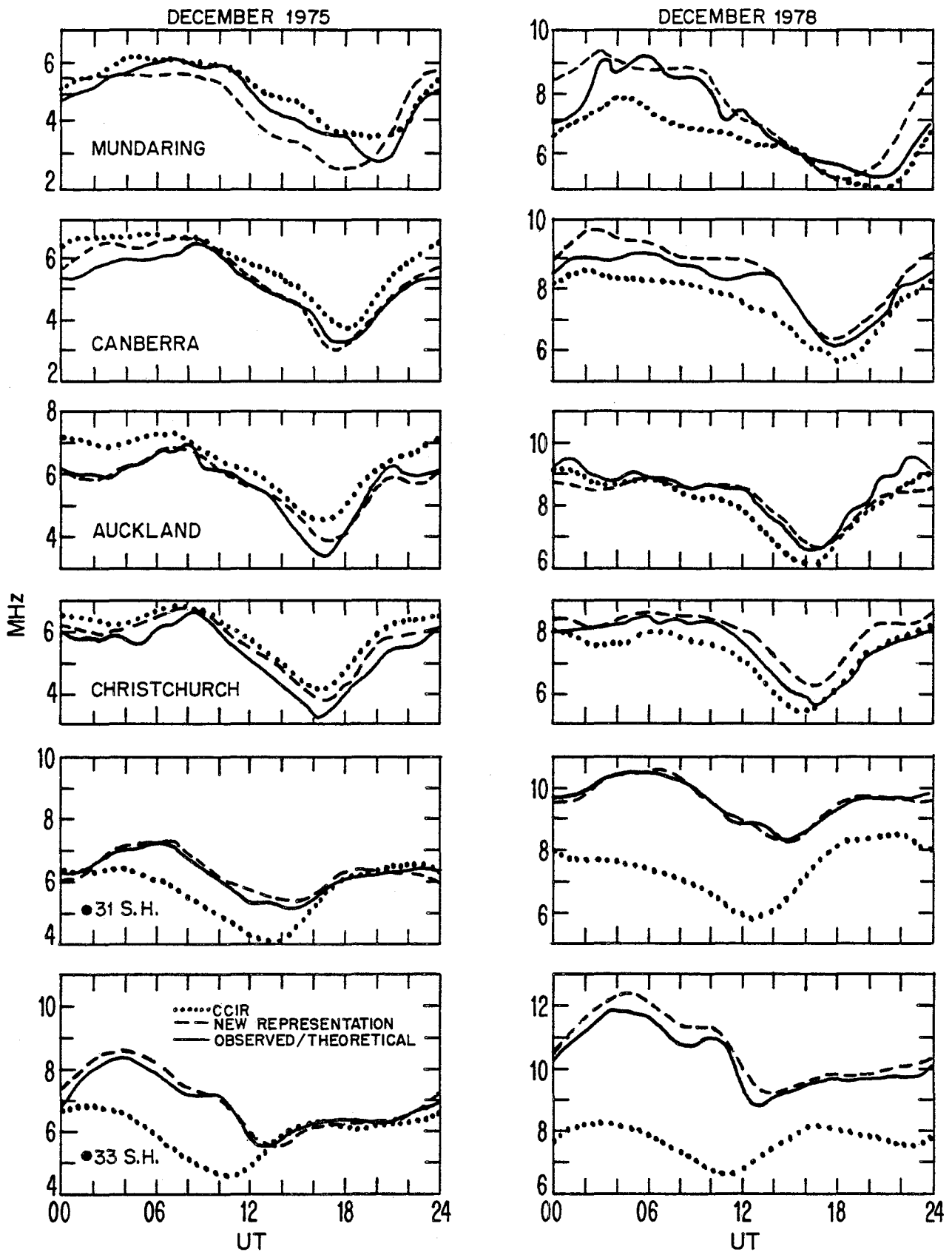


Figure 15. Comparison between the diurnal variation of foF2 for December 1975 and December 1978 deduced from the existing CCIR coefficients, the new coefficients developed in this study, and from the theoretical model or from observations where available. Plots are shown for observations at Mundaring, Canberra, Auckland and Christchurch and theoretical calculations at points 31 and 33.

Table 3: Location of A stations and D points
used to illustrate
diurnal behavior of foF2

Station/Point	Geog.Lat (°S)	Geog.Long (°E)	Declination (°E)	Modified Dip (°N)
Brisbane, Australia	27.5	152.9	12	-47
Norfolk Island, Australia	29.0	168.0	15	-47
Port Stanley, Falkland Island	51.7	300.0	7	-47
Mundaring, Australia	320.0	116.31	- 2.5	-52
Canberra, Australia	35.3	149.0	12	-52
Auckland, New Zealand	37.0	173.0	20	-51
Christchurch, New Zealand	43.6	172.8	22	-55
Kerguelen, Indian Ocean	49.4	70.3	-50	-56
Hobart, Tasmania	42.9	147.3	12	-56
Campbell Island, New Zealand	52.5	169.2	30	-59
Argentine Island	65.2	295.7	17	-58
16 S.H.	34.0	207.0	14	-47
19 S.H.	43.0	262.0	22	-46
20 S.H.	43.0	340.0	-23	-49
31 S.H.	47.0	217.0	25	-53
33 S.H.	54.0	257.0	32	-54
57 S.H.	47.0	100.0	-45	-58
60 S.H.	60.0	205.0	40	-61

this figure for which foF2 observations were available and were used in the new analysis, the new representation is at least as good and in most instances better than that obtained from the CCIR coefficients. The theoretical points shown in this figure are located in the South Pacific, and the discrepancies between the theoretical points and the representation from the CCIR coefficients is even greater than that observed in Figure 14.

The set of stations in Figure 16 illustrates what has for many years been an apparent contradiction in the expected diurnal variation of foF2 in the Southern Hemisphere. In comparing the diurnal variation of foF2 observations at Kerguelen with those at Argentine Island, the diurnal variations appear almost to display the same temporal behavior. But, in fact, although the maximum value of foF2 occurs at UT 0700 at both Kerguelen and Argentine Island in December 1978, the local time at Kerguelen is 1200, while at Argentine Island it is 0300. A possible explanation for this is the effect of the declination of the magnetic field and the influence of the neutral air wind in moving ionization along the field lines. Kerguelen has a westward declination, and Argentine Island has an eastward declination. This same declination effect is obvious in the diurnal curves for the other stations and the theoretical points, shown in Figure 16. Both Kerguelen and the point 57 have a western declination. Hobart, Campbell Island, and point 60 all have an eastward declination. The very low nighttime foF2 values for point 57 are substantiated by those observed at Kerguelen. Similarly, the very high nighttime foF2 values for point 60 are in good agreement with those observed at Campbell Island and Argentine Island in both 1975 and 1978. Locations for which the declination is eastward have larger nighttime values of foF2 than do locations with westward declinations. This is because the zonal wind for December blows eastward in the night hours (see Figure 2 for the December 1978 wind pattern). The eastward blowing zonal wind lifts ionization up the field lines at locations having an eastward declination. The ionization is thus raised to a region where the loss rate is less, hence the value of foF2 is raised. The eastward zonal wind forces ionization down the field lines at locations having westward declinations. The ionization is therefore forced to regions of increased loss rate resulting in lower values of foF2.

The locations in Figures 14 through 16 for which observed values of foF2 were available were used to determine the difference between the respective mapped values and the observed values. The difference between foF2 deduced from the CCIR coefficients and the observed values and the difference between foF2 deduced from the new analysis (using the theoretical model) and observations of foF2 were

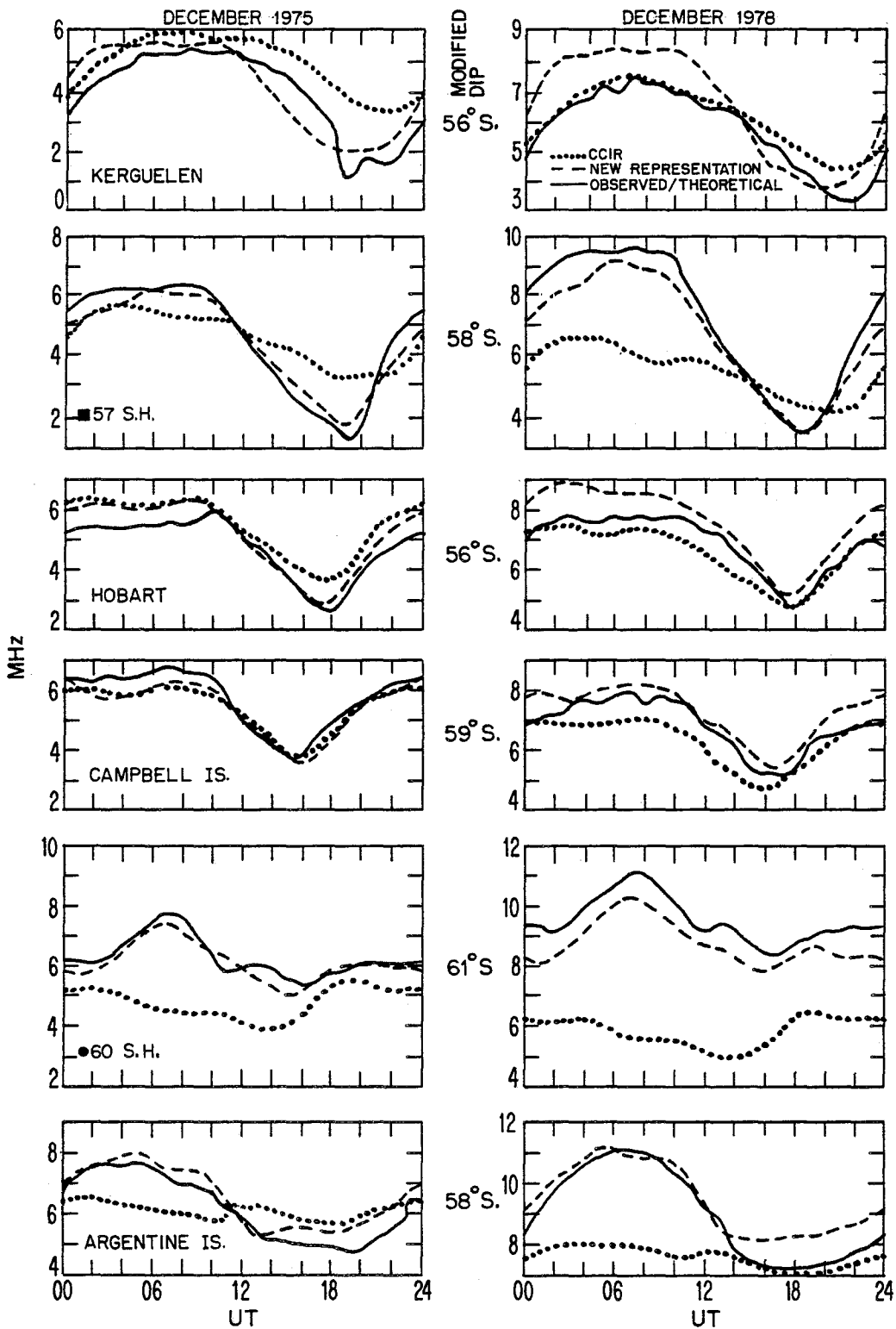


Figure 16. Comparison between the diurnal variation of foF2 for December 1975 and December 1978 deduced from the existing CCIR coefficients, the new coefficients developed in this study, and from the theoretical model or from observations where available. Plots are shown for observations at Kerguelen, Hobart, Campbell Island, and Argentine Island and theoretical calculations at points 57 and 60.

computed and averaged over the entire 24 hour period at each location. It was found that during December 1975 the average difference between observed values of foF2 and those determined from the CCIR coefficients for all locations taken together was 14 percent. The average difference between the observed values of foF2 and those determined from the new analysis was eight percent in December 1975. For the December 1978 data, it was found that both the CCIR coefficients and the new analysis containing the theoretical data yield differences on the order of seven percent.

Figure 17 shows comparisons between foF2 obtained using the CCIR coefficients and foF2 obtained from the new analysis for the months of July 1975 and September 1978. The four locations illustrated are all in ocean areas where no observations are available. It is obvious from the figure that the diurnal variation of foF2 determined from the maps derived using the theoretical values of foF2 yield different representations than do the CCIR coefficients. This is not too surprising in light of the foregoing discussion. The values of foF2 deduced from the CCIR coefficients at the points illustrated in Figure 17 were obtained as the result of extrapolating land-based observations without regard for magnetic declination effects. Referring back to Figure 6, it is seen that points 19, 31, and 60 all have eastward declinations, while point 20 has a westward declination. The effects of the neutral-air wind are to lower the daytime values of foF2 at the locations having eastward declinations while tending to raise the nighttime values at the same locations. The results for September 1978 show that differences on the order of 4 MHz between foF2 derived from the CCIR coefficients and from the new analysis undertaken in this study are possible. Using values of foF2 that differ by 4 MHz in HF propagation prediction programs would lead to differences in the calculated one-hop maximum usable frequency for a 3000 km path of about 12 MHz.

5. DISCUSSION AND CONCLUSION

There have been a number of studies directed toward determining the accuracy of the existing maps of foF2. Many of these (King and Slater, 1973; Wakai and Matuura, 1980, for example) have been directed toward comparing the values determined from the existing maps with average values of foF2 determined from satellite data. Studies have also been undertaken (Rush and Edwards, 1976; Flattery and Ramsay, 1975) to develop methods to specify the global distribution of foF2 on an hourly basis. All these studies rely upon the monthly median maps of foF2 determined from the CCIR coefficients. The values of foF2 predicted from these coefficients have been found to agree well with observations at those locations for which

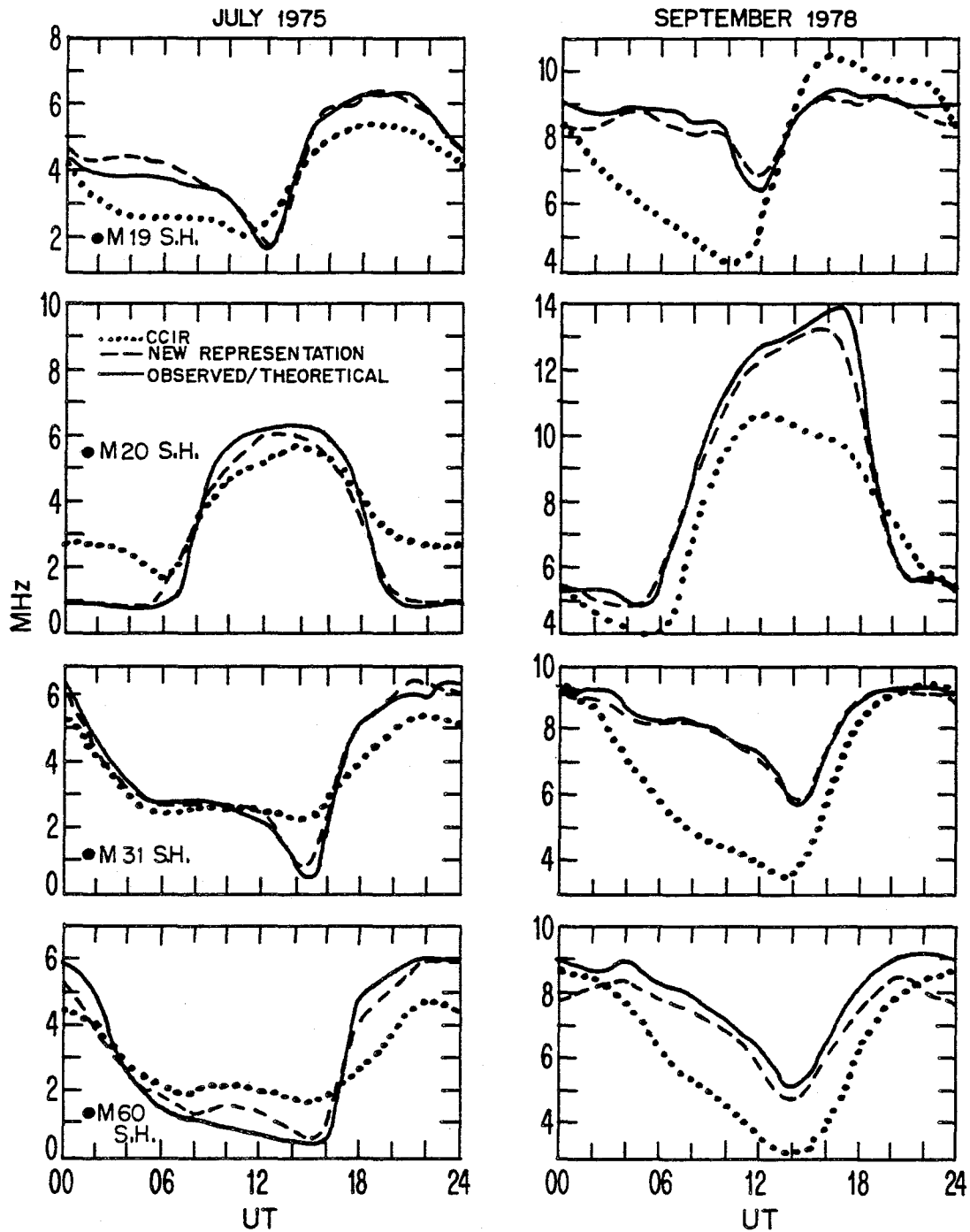


Figure 17. Comparison between the diurnal variation of foF2 for July 1975 and September 1978 deduced from the existing CCIR coefficients, the new coefficients developed in this study, and from the theoretical model for points 19, 20, 31, and 60.

data were used in the development of the coefficients. However, at regions of the globe that are inaccessible to routine ionospheric sounding, the agreement is less than optimum. The incorporation of theoretically derived values of the F2 region critical frequency into the numerical ionospheric mapping scheme has been shown to lead to improvements in maps of foF2 at middle latitudes. Comparing values of foF2 derived from the existing CCIR coefficients with those derived from the new analysis undertaken in this study has revealed that improvements in the global representation of foF2 have been achieved. This is due primarily to the fact that, in the current study, values of foF2 in locations for which observations were not available were determined using a model of the ionospheric electron density that incorporates the physical mechanisms responsible for the distribution of ionization in the ionosphere. The existing CCIR coefficients, on the other hand, were deduced by extrapolating available observations of foF2 into inaccessible regions, accounting only for the magnetic inclination control of the F2 region. The current study has permitted both inclination and declination effects to be incorporated into the generation of the global maps of foF2. The fact that the results of the current study show drastic improvement in the maps in regions of the Southern Hemisphere, where observations are not available to routine procedures, is particularly important.

The ionospheric F2 region in the Southern Hemisphere was emphasized in this study because of the large areas where normal ionospheric sounding is impossible due to obvious geographical considerations. Because the Northern Hemisphere observations of foF2 are more numerous, and the regions for which data are generally unavailable are not as large in geographical extent, improvements in the representation in the Northern Hemisphere foF2 may not be as dramatic as those of the Southern Hemisphere. In fact, this is exactly what has been found by conducting a study for the Northern Hemisphere similar to that described in Section 4 for the Southern Hemisphere.

The results presented in this report have been confined to the middle latitude ionosphere. Calculations of foF2 using the time-dependent continuity equation were also performed for selected low latitude locations. Because of the steep latitudinal gradients in foF2 in the vicinity of the equatorial anomaly, numerous theoretical calculations are needed to provide input into the mapping procedure. A preliminary analysis performed on the low latitude results has indicated the need for additional theoretical calculations so that realistic maps of the ionosphere structure at equatorial latitudes can be obtained. It is anticipated that because of the large regions of the globe in the equatorial latitudes that are not

accessible to routine observation, the improvement in the global maps of foF2 resulting from incorporation of the theoretical values would be comparable to that shown in Section 4. Such a study should be undertaken.

A completely new set of coefficients that can be used to determine the F2 region critical frequency on a global scale should be developed in order to incorporate all the improvements that are possible. In order to accomplish this, it will be necessary to extend the current study to include other months of the year to obtain the proper seasonal behavior of foF2 can be obtained. An improved representation of foF2 at high latitudes, coupled with values determined from the theoretical model for low latitudes, can lead to a much better overall representation of the global maps of foF2. This improvement would then be directly manifested in comparable improvements in all models of the ionospheric structure and radio propagation conditions that rely upon maps of foF2.

6. ACKNOWLEDGMENT

The authors are most grateful for the support and assistance provided by Mrs. Jane Perry, Department of Defense, during the course of this study.

7. REFERENCES

- Anderson, D. N. (1973), A theoretical study of the ionosphere F region equatorial anomaly - I. Theory, *Plan. Space Sci.* 21, 409-419.
- Barghausen, A. F., J. W. Finney, L. L. Proctor, and L. D. Schultz (1969), Predicting long-term operational parameters of high-frequency sky-wave telecommunications systems, ESSA Technical Report, ERL-110-ITS-78.
- Bent, R. B., J. R. Lepofsky, S. K. Llewellyn, and P. G. Schmid (1978), Ionospheric range-rate effects in satellite-to-satellite tracking, in AGARD Conference Proceedings No. 230 Operational Modelling of the Aerospace Propagation Environment, Vol. I, edited by H. Soicher, 9-1 - 9-15, Ottawa, Canada.
- Bergthorsson, P., and B. R. Doos (1955), Numerical weather map analysis, *Tellus* 7, 329-340.
- CCIR (1978a), Report 340-3, CCIR Atlas of ionospheric characteristics, Recommendations and Reports of the CCIR, 1978, Vol. VI, Kyoto.

- CCIR (1978b), Supplement to Report 252-2, Second CCIR computer-based interim method for estimating sky-wave field strength and transmission loss at frequencies between 2 and 30 MHz, Recommendations and Reports of the CCIR, 1978, Vol. VI, Kyoto.
- Crank, J. and P. Nicolson (1947), A practical method for numerical evaluation of solutions of partial differential equations of the heat-conductor type, *Cam. Phil. Soc. Math. Proc.* 43, 50-67.
- Crow, E. L., and D. H. Zacharisen (1960), The error in prediction of F2 maximum usable frequencies by world maps based on sunspot number, Proceedings of Symposium on Statistical Methods in Radio Wave Propagation, University of California, Los Angeles, (edited by W. C. Hoffman, Symposium Publications Division, Pergamon Press, New York).
- Flattery, T. W., and A. C. Ramsay (1975), Derivation of total electron content for real-time global application, Proceedings of the Symposium of the Effects of the Ionosphere on Space Systems and Communications, (edited by J. H. Goodman), 336-344, U. S. Government Printing Office, Washington, D. C.
- Hedin, A. E., C. A. Reber, G. P. Newton, N. W. Spencer, H. C. Briston, H. B. Mayer, and W. E. Potter (1977), A global thermospheric model based on mass spectrometer and incoherent scatter data, *J. Geophys. Res.* 82, 2148-2156.
- Jones, W. B., and R. M. Gallet (1962), The representation of diurnal and geographic variations of ionospheric data by numerical methods, *Telecommun. Jour.*, 29, 129-149.
- Jones, W. B., and D. L. Obitts (1970), Global representation of annual and solar cycle variation of foF2 monthly median 1954-1958, Office of Telecommunications Research Report, OT/ITS RR3, (NTIS Access. No. COM 75-11143/AS).
- Jones, W. B., R. P. Graham, and M. Leftin (1969), Advances in ionospheric mapping by numerical methods, ESSA Technical Report ERL-107-ITS-75.
- Kendall, P. C., and W. M. Pickering (1967), Magnetoplasma diffusion at F2-region altitudes, *Plan. Space Sci.* 15, 825-833.
- King, J. W., and A. J. Slater (1973), Errors in predicted values of foF2 and hmF2 compared with the observed day-to-day variability, *Telecommun. Journ.* 40, 766.
- Leftin, M. (1976), Numerical representation of monthly median critical frequencies of the regular E region (foE), Office of Telecommunications Report 76-88, (NTIS Access. No. PB 255-484/AS).
- Matuura, N. (1979), Atlas of ionospheric critical frequency (foF2) obtained from Ionospheric Sounding Satellite-Observation, Part 1, August to December 1978, Radio Research Laboratories of Japan, March.

- Nisbet, J. S. (1971), On the construction and use of a simple ionospheric model, *Radio Sci.* 6, 437-464.
- Rosich, R. K., and W. B. Jones (1973), The numerical representation of the critical frequency of the F1 region of the ionosphere, Office of Telecommunications Report 73-22, (NTIS Access. No. 75-10813/AS).
- Rush, C. M. (1978), An ionospheric observation network for use in short-term propagation predictions, *Telecommun. Jour.* 43, 544-549.
- Rush, C. M., and W. R. Edwards (1976), An automated mapping technique for representing the hourly behavior of the ionosphere, *Radio Sci.* 11, 931-937.
- Rush, C. M., and J. Gibbs (1973), Predicting the day-to-day variability of the mid-latitude ionosphere for application to HF propagation predictions, Air Force Cambridge Research Laboratories Technical Report, TR-73-0335, Defense Documentation Center, Alexandria, VA.
- Stern, D. (1965), Classification of magnetic shells, *J. Geophys. Res.* 70, 3629-3634.
- Stern, D. (1967), Geomagnetic euler potentials, *J. Geophys. Res.* 72, 3995-4005.
- Vestine, E. H., L. Laporte, I. Large and W. E. Scott (1947), *The Geomagnetic Field, Its Description and Analysis*, (Carnegie Inst. of Washington Publication 580, Washington, D. C.).
- Wakai, N., and N. Matuura (1980), Operation and experimental results of the Ionosphere Sounding Satellite-b, *Acts Astronautica* 7, 999-1020.
- Woodman, R. (1970), Vertical drift velocities and east-west electric fields at the magnetic equator, *J. Geophys. Res.* 31, 6249-6259.
- Zevakina, R. A., Ye. V. Lavrova, and L. N. Lyakhova (1967), *Manual on short-term prediction of ionospheric geomagnetic storms and radio-propagation forecasting service (in Russia)*, (Published by Nauka, Moscow).

BIBLIOGRAPHIC DATA SHEET

		1. PUBLICATION NO. NTIA Report 82-93	2. Gov't Accession No.	3. Recipient's Accession No.
4. TITLE AND SUBTITLE THE USE OF THEORETICAL MODELS TO IMPROVE GLOBAL MAPS OF foF2			5. Publication Date January 1982	6. Performing Organization Code NTIA/ITS
7. AUTHOR(S) Charles M. Rush, Margo PoKempner, David N. Anderson, and F. G. Stewart			9. Project/Task/Work Unit No.	
8. PERFORMING ORGANIZATION NAME AND ADDRESS U. S. Department of Commerce National Telecommunications and Information Administration Institute for Telecommunication Sciences Boulder, Colorado 80303			10. Contract/Grant No.	
11. Sponsoring Organization Name and Address Same			12. Type of Report and Period Covered	
			13.	
14. SUPPLEMENTARY NOTES				
15. ABSTRACT (A 200-word or less factual summary of most significant information. If document includes a significant bibliography or literature survey, mention it here.) In this report, the results of a study to improve the global maps of monthly median values of the F2 region critical frequency, foF2, using values determined from a theoretical model, are presented. The object of the study was to obtain values of the mid-latitude F-region critical frequency which could be used to improve the prediction of ionospheric parameters in regions of the earth inaccessible to ground-based measurements. This was accomplished by including, into the theoretical calculations, realistic physical processes along with a realistic geomagnetic field model. Parameters were adjusted so that agreement was achieved between calculated and observed foF2 values as a function of local time at different stations and then these same input parameters (i.e., neutral wind field, neutral atmospheric model, electrodynamic drift) were assumed valid at all regions of interest where the major difference is the gemagnetic field-line configuration. Coefficients that yield global representations of foF2 were then determined using the theoretically derived foF2 values, and the predicted <u>critical frequencies compared with observed values to estimate the degree of</u> improvement. F2, ionospheric mapping, neutral winds, time-dependent continuity equation				
16. Key Words (Alphabetical order, separated by semicolons)				
17. AVAILABILITY STATEMENT <input checked="" type="checkbox"/> UNLIMITED. <input type="checkbox"/> FOR OFFICIAL DISTRIBUTION.		18. Security Class. (This report) Unclassified		20. Number of pages 46
		19. Security Class. (This page) Unclassified		21. Price:

